Version 2: Algorithm Theoretical Basis Document

Aquarius Salinity Retrieval Algorithm

Frank J. Wentz and David M. Le Vine

1 Introduction 3
2 The Forward Model 3
2.1 The Antenna Temperature Equation 3
2.2 Radiation from Space 6
2.2.1 Direct Galactic Radiation 6
2.2.2 Reflected Galactic Radiation 7
2.2.3 Direct Solar Radiation 9
2.2.4 Reflected Solar Radiation 9
2.2.5 Backscattered Solar Radiation 10
2.2.6 Reflected Lunar Radiation 11
2.3 Earth-Only T_B Equation 12
2.3.1 Theoretical Formulation 12
2.3.2 Empirical Approach to Specifying Atmospheric Terms 13
2.3.3 Empirical Approach to Specifying Emissivity 14
2.3.4 Empirical Approach to Specifying Reflected and Scattered Radiation 15
2.3.5 Empirical Approach to Handling Land and Sea-Ice Observations 15
3 Salinity Retrieval Algorithm 15
3.1 Removal of the Radiation Coming from Space 16
3.2 Definition of Reference Brightness Temperature 16
3.3 Estimation of Top-of-the-Ionosphere Brightness Temperature 17
3.4 Correction for Faraday Rotation 18
3.5 Removal of Atmospheric Effects 19
3.6 Estimation of Salinity Given Surface Emission Brightness Temperature 20
3.7 Calculation of Expected Antenna Temperature 21
3.8 Correction for Land Entering the Antenna Sidelobes 22
4 Outstanding Issues 22
5 References 22
6 Appendix A. Reflected Galactic Brightness Temperature 27
7 Appendix B. Land and Sea-Ice Reflectivities 30

8. Appendix C: Dielectric Constant of Soil 36
9. Appendix D: Gain Coefficient for Reflected Lunar Radiation 45

Version 2: Algorithm Theoretical Basis Document

Aquarius Salinity Retrieval Algorithm: Final Pre-Launch Version

Frank J. Wentz and David M. Le Vine

1. Introduction

This document provides the theoretical basis for the Aquarius salinity retrieval algorithm. The inputs to the algorithm are the Aquarius antenna temperature (T_A) measurements along with a number of NCEP operational products and pre-computed tables of space radiation coming from the galaxy and sun. The output is sea-surface salinity and many intermediate variables required for the salinity calculation. This is the pre-launch version of the ATBD. Changes made post-launch will be included as addenda and updated periodically. In particular, the roughness correction is based on pre-launch information and changes are likely as soon as data from the scatterometer become available.

The ATBD is organized into two main sections. The Forward Model Section describes how the Aquarius antenna temperature is calculated given the following information:

1. Footprint location: time, latitude, and longitude;
2. Pointing angles: Earth incidence and azimuth angles; sun and moon pointing vectors;
3. Antenna pattern;
4. NCEP operational fields: surface temperature and vector wind, atmospheric profiles (pressure, temperature, humidity, liquid water), sea ice;
5. Solar flux values from radio astronomy observations;
6. Pre-computed tables giving the T_A contribution of the galaxy and sun (moon contribution is computed from an analytic expression).

The Retrieval Algorithm Section describes how the various components of the forward model are used to estimate salinity given the Aquarius T_A measurement. The algorithm is essentially a subtraction process in which the unwanted sources of radiation (galaxy, sun, moon, and Earth's atmosphere) are removed from the T_A measurement in order to obtain just the Earth's surface emission term. A simple regression is then used to estimate salinity from the surface emission.

2. The Forward Model

The forward model gives the Aquarius antenna temperature in terms of the antenna pattern G convolved with the surrounding brightness temperatures (T_B) 4π-steradian field. The convolution of G with T_B is called the antenna temperature equation. The field of surrounding brightness temperatures is partitioned into a space segment and an Earth segment (Le Vine et al, 2011).

2.1 The Antenna Temperature Equation

In this subsection, we work in terms of the classical, rather than the modified, Stokes parameters (i.e. Stokes parameters in brightness temperature, Randa et al, 2008). The measurement vector $\mathbf{T}_{A,mea}$, which is called the antenna temperature vector, is then defined as:

$$\mathbf{T_A}_{.mea} \equiv \begin{bmatrix} T_{A1,mea} \\ T_{A2,mea} \\ T_{A3,mea} \\ T_{A4,mea} \end{bmatrix} = \begin{bmatrix} T_{Amea,V} + T_{Amea,H} \\ T_{Amea,V} - T_{Amea,H} \\ T_{Amea,+45} - T_{Amea,-45} \\ T_{Amea,left} - T_{Amea,right} \end{bmatrix} \tag{1}$$

where $T_{Amea,V}$, $T_{Amea,H}$, $T_{Amea,+45}$, $T_{Amea,-45}$, $T_{Amea,left}$, and $T_{Amea,right}$ are the v-pol, h-pol, plus 45°, minus 45°, left circular, and right circular polarization measurements. Aquarius will only measure $T_{Amea,V}$, $T_{Amea,H}$, $T_{Amea,+45}$, and $T_{Amea,-45}$, (Le Vine et al, 2007b) but the full Stokes formulation is included here for completeness. Likewise, brightness temperatures are defined as

$$\mathbf{T_B} \equiv \begin{bmatrix} T_{B1} \\ T_{B2} \\ T_{B3} \\ T_{B4} \end{bmatrix} = \begin{bmatrix} T_{B,V} + T_{B,H} \\ T_{B,V} - T_{B,H} \\ T_{B,+45} - T_{B,-45} \\ T_{B,left} - T_{B,right} \end{bmatrix} \tag{2}$$

The measurements represent an integration over the entire 4π steradians surrounding the antenna. We divide this integration into 2 components: the Earth field of view and the space field of view.

$$\mathbf{T_A}_{,mea} = \mathbf{T_A}_{,earth} + \mathbf{T_A}_{,space} \tag{3}$$

$$\mathbf{T_A}_{,earth} = \frac{1}{4\pi} \int_{Earth} \mathbf{G}(\mathbf{b}) \; \mathbf{\Psi}(\phi) \; \mathbf{T_B}_{,toa} \frac{\partial \Omega}{\partial A} dA \tag{4}$$

$$\mathbf{T_A}_{,space} = \frac{1}{4\pi} \int_{Space} \mathbf{G}(\mathbf{b}) \mathbf{T_B}_{,space} d\Omega \tag{5}$$

The first integral is over the surface of the earth, where the differential surface area is dA. The second integral is over space, where $d\Omega$ is the differential solid angle. The matrix **G** is a 4×4 matrix describing the antenna gain function (see Le Vine et al, 2007a for an example of the gain matrix in the case of the modified Stokes parameters). Each element in this matrix is a function of the look direction **b.** For the first integral, **b** is the unit vector pointing from the antenna to dA. For the second integral, **b** is the unit vector in the direction specified by $d\Omega$.

The term $\mathbf{\Psi}(\phi)$ in (4) is a rotation matrix defined by

$$\mathbf{\Psi}(\phi) = \begin{bmatrix} 1 & 0 & 0 & 0 \\ 0 & \cos 2\phi & -\sin 2\phi & 0 \\ 0 & \sin 2\phi & \cos 2\phi & 0 \\ 0 & 0 & 0 & 1 \end{bmatrix} \tag{6}$$

The rotation angle ϕ is the sum of the antenna polarization angle ϕ_{ant} and Faraday rotation angle ϕ_f due to the ionosphere: $\phi = \phi_{ant} + \phi_f$. The angle ϕ_{ant} is the angle between the polarization vectors defined at the antenna and the polarization vectors defined for radiometry at the Earth surface. It is an implicit function of **b** as well as the attitude of the Aquarius spacecraft. The Faraday rotation angle ϕ_f is a function of **b** as well as the Earth's magnetic field vector **B** and the electron density along the path **b**.

$$\phi_f = \frac{1.35493\times10^{-5}}{\nu^2} N_e\left(-\mathbf{b}\cdot\mathbf{B}\right)\frac{\partial b}{\partial h} \tag{7}$$

where ν is frequency in GHz, N_e is vertically-integrated electron counts in TEC units, **B** is the Earth's magnetic field vector in nanotesla units at the mean height of the ionosphere, and the last term is the partial derivative of slant range to the vertical height, which converts N_e from a vertically-integrated value to a slant-range integrated value (e.g. Le Vine and Abraham, 2002). The rotation matrix is not required for the space integration because we assume the space radiation is unpolarized.

The ratio of the differential solid angle to the differential surface area is

$$\frac{\partial\Omega}{\partial A} = f_{lat}\frac{\cos\theta_i}{r^2} \tag{8}$$

where θ_i is the incidence angle and r is the range. For a spherical Earth, the leading term f_{lat} would be unity. However, the Earth is modeled as an oblate spheroid and as a consequence this term is a function of latitude, deviating about ±1% from unity.

The brightness temperature vector for Earth in equation (4) is

$$\mathbf{T}_{\mathbf{B},toa} = \begin{bmatrix} T_{BV,toa} + T_{BH,toa} \\ T_{BV,toa} - T_{BH,toa} \\ 0 \\ 0 \end{bmatrix} \tag{9}$$

where $T_{BV,toa}$ and $T_{BH,toa}$ are the v-pol and h-pol Earth brightness temperatures measured at the top of the atmosphere (TOA), but below the ionosphere. We have assumed that the 3rd and 4th Stokes parameters coming from the Earth are negligibly small at 1.4 GHz.

The brightness temperature vector for space is

$$\mathbf{T}_{\mathbf{B},space} = \begin{bmatrix} 2T_{Bspace} \\ 0 \\ 0 \\ 0 \end{bmatrix} \tag{10}$$

The space contribution consists of cosmic background radiation, galactic radiation, and direct rays from the sun and the moon. We assume the space radiation is unpolarized in which case only the 1st Stokes parameter is non-zero (but this is an assumption which needs to be investigated). Section 2.2 discusses this space contribution in more detail.

The Earth's limb also contributes to the radiation received by the antenna. The Earth's limb varies from 260 K at the surface to 11 K at 10 km. Above 40 km, the limb brightness temperature is less than 0.001 K. When integrated over the antenna pattern, the limb contributes only 0.006 K to the 1st Stokes and is essentially zero for the 2nd through 4th Stokes.

At this point in our analysis, we drop the 4th Stokes from the notation. Aquarius does not measure the 4th Stokes, and it does not need to be considered. So hereafter, all T_A and T_B vectors now have just 3 components, and the antenna gain matrix and rotation matrix are 3 by 3.

2.2 Radiation from Space

Space radiation consists of cosmic background (2.73 K), galactic, solar, and lunar components. This radiation is received by the antenna in two ways: directly and via Earth reflection and scattering. The contribution of direct lunar radiation is completely negligible (lunar radiation is a factor of 10^{-4} less than the solar radiation). However, lunar radiation reflecting off the ocean surface is not negligible because at certain times each month the reflected ray enters the antenna mainbeam (Dinnat et al, 2009).

These space radiation terms are denoted by:

1. Direct and reflected galactic radiation: $\mathbf{T}_{\mathbf{A},gal\_dir}$ and $\mathbf{T}_{\mathbf{A},gal\_ref}$
2. Direct, reflected, and backscatter solar radiation: $\mathbf{T}_{\mathbf{A},sun\_dir}$, $\mathbf{T}_{\mathbf{A},sun\_ref}$, and $\mathbf{T}_{\mathbf{A},sun\_bak}$
3. Reflected lunar radiation: $\mathbf{T}_{\mathbf{A},mon\_ref}$

Because the solar radiation is so intense, one must consider both the specular reflected component that enters the far sidelobes of the antenna and the backscatter component that enters the mainbeam of the antenna which can occur at certain times of the year when the main beam is not in darkness (Dinnat and Le Vine, 2008).

Given these 6 terms, equations (4) and (5) can be partitioned as

$$\mathbf{T}_{\mathbf{A},earth} = \mathbf{T}_{\mathbf{A},earth\_dir} + \mathbf{T}_{\mathbf{A},gal\_ref} + \mathbf{T}_{\mathbf{A},sun\_ref} + \mathbf{T}_{\mathbf{A},sun\_bak} + \mathbf{T}_{\mathbf{A},mon\_ref} \tag{11}$$

$$\mathbf{T}_{\mathbf{A},space} = \mathbf{T}_{\mathbf{A},gal\_dir} + \mathbf{T}_{\mathbf{A},sun\_dir} \tag{12}$$

where the new term $\mathbf{T}_{\mathbf{A},earth\_dir}$ refers to radiation coming just from the earth (i.e., no space radiation reflections). It is better to directly compute the antenna temperatures of the space reflections by numerically performing the required integrations rather than trying to model them as brightness temperature components reflected off the earth. For example, one could model the reflected galactic radiation as one component of $\mathbf{T}_{\mathbf{B},toa}$ in (4). However, the antenna pattern correction discussed in Section 3.3 works best for a smoothly varying brightness temperature scene. The galactic radiation field has very sharp features that would present a problem for the APC. Therefore, it was decided to numerically compute the antenna temperatures for the various space reflections and store the results of the integrations as tables. The next subsections describe how the 6 space terms are computed.

2.2.1 Direct Galactic Radiation

The direct galactic radiation $\mathbf{T}_{\mathbf{A},gal\_dir}$ is computed by numerically evaluating the integral in (5),

$$\mathbf{T}_{\mathbf{A},gal\_dir} = \frac{1}{4\pi} \int_{Space} \mathbf{G}(\mathbf{b}) \mathbf{T}_{\mathbf{B},gal} d\Omega \tag{13}$$

$$\mathbf{T}_{\mathbf{B},gal} = \begin{bmatrix} 2T_{Bgal} \\ 0 \\ 0 \end{bmatrix} \tag{14}$$

where T_{Bgal} comes from a galactic map [*Le Vine and Abraham*, 2004] that has the cosmic background radiation of 2.73K added in. The pixel size in the LeVine-Abraham map is

0.25^0x0.25^0, and the minimum pixel value is about 3K. We interpret the 3 K floor of the galactic map as the cosmic background radiation (2.73 K) plus radiation coming from distant galaxies.

The computation of $\mathbf{T}_{\mathbf{A},gal\_dir}$ depends on the orbit position of the satellite and on the time of year as the Aquarius orbit precesses relative to the fixed galaxy every sidereal year (365.25636 days). A separate computation is done for each of the 3 radiometers because the antenna patterns are different. Tables of $\mathbf{T}_{\mathbf{A},gal\_dir}$ are generated for 1441 positions within an orbit (every ¼°) and for 1441 periods during a sidereal year (about every 6 hours). These tables are specified by tagal_dir_tab(1441,1441,3,3), where the 4 dimensions correspond to time of sidereal year, orbit position, Stokes number, and radiometer number. Time is referenced to January 1, 2010, 0Z, and orbit position is referenced to the South Pole node. The South Pole node is the point in the orbit where the polar component of spacecraft velocity vector changes from pointing south to pointing north. The orbit position is the angle between a vector pointing from the Earth center to the South Pole node and a vector pointing from the Earth's center to the current position of the satellite. For example, 90° would correspond approximately to the satellite crossing the equator going south to north. The periodicity of the time variable is one sidereal year (365.25636 days). Even though it is assumed that the galactic T_B is unpolarized, antenna polarization mixing results in $\mathbf{T}_{\mathbf{A},gal\_dir}$ having all four Stokes components. $\mathbf{T}_{\mathbf{A},gal\_dir}$ is a small (0.3K), slowly varying term and the granularity size of the table is more than sufficient. During operational processing a bi-linear interpolation is used to look up tagal_dir_tab as a function of orbit position and time of year.

The calculation of $\mathbf{T}_{\mathbf{A},gal\_dir}$ depends upon the assumed ascending equator crossing time for Aquarius. A value of 5:59:59.16 pm was used to generate the table tagal_dir_tab. If the actual ascending node time is different, the relative phase of the table can be adjusted via an input constant orbit_phase_dif that specifies the actual node time relative to 6:00:00 pm. Currently orbit_phase_dif is set to -0.84 seconds, and it will be revised after launch to the true value.

2.2.2 Reflected Galactic Radiation

The reflected galactic radiation $\mathbf{T}_{\mathbf{A},\mathrm{gal\_ref}}$ is the most difficult space term to deal with. It can be large (5 K), have sharp features, and be modulated by the ocean surface roughness. To calculate $\mathbf{T}_{\mathbf{A},gal\_ref}$, an integration over the Earth is done as follows

$$\mathbf{T}_{\mathbf{A},gal\_ref} = \frac{1}{4\pi}\int_{Earth} \mathbf{G}(\mathbf{b}) \quad (\phi) \quad _{\mathbf{B},gal\_ref} \frac{\partial\Omega}{\partial A} dA \tag{15}$$

where $\mathbf{T}_{\mathbf{B},gal\_ref}$ is the brightness temperature of the reflected galactic radiation at the top of the atmosphere. For a specular surface, and since the background radiation is unpolarized, the reflected galactic radiation can be written as

$$\mathbf{T}_{\mathbf{B},gal\_ref} = \tau^2 \left(T_{Bgal} - T_{B\cos}\right)\mathbf{R} \tag{16}$$

$$\mathbf{R} = \begin{bmatrix} R_V + R_H \\ R_V - R_H \\ 0 \end{bmatrix} \tag{17}$$

where τ is the atmospheric transmittance and the vector **R** is the reflectivity for the 1st and 2nd Stokes in terms of the v-pol and h-pol reflectivity. As shown in Equation (16) the constant, T_{Bcos} = 3K, is subtracted from the galactic background before computing the reflected galactic radiation. Because T_{Bcos} is essentially constant in space it is convenient to include it in the Earth radiation calculation (see Section 2.3). Note that T_{Bcos} is actually the cosmic background (2.73 K) plus a constant (0.37 K) representing a mean "floor" of the celestial background radiation.

The approach outlined above in (16) only accounts for galactic reflections in the specular direction. In actuality, bistatic scattering from a rough ocean will scatter galactic radiation from many different directions into the mainlobe of the antenna. In effect, a rough ocean surface tends to add additional spatial smoothing to $\mathbf{T}_{\mathbf{A},gal\_ref}$. The formulation for $\mathbf{T}_{\mathbf{B}}$,gal_ref for a rough ocean surface is given in Appendix A.

Tables of $\mathbf{T}_{\mathbf{A},gal\_ref}$ are made. As was the case for the direct galactic radiation, $\mathbf{T}_{\mathbf{A},gal\_ref}$ depends on the orbit position of the satellite and on the time of year. The tables have the same structure and format as the $\mathbf{T}_{\mathbf{A},gal\_dir}$ except that one additional dimension is included for wind speed. The tables have the form tagal_ref_tab(1441,1441,3,3,5), where the first four dimensions are the same as described above for $\mathbf{T}_{\mathbf{A},gal\_dir}$. The 5th dimension is wind speed going from 0 to 20 m/s in 5 m/s steps.

When computing tagal_ref_tab(1441,1441,3,3,5), the atmospheric transmittance τ is set to unity and the reflectivities R_V and R_H are set to ocean reflectivity values corresponding to a surface temperature and salinity of 20°C and 35 psu, respectively, and wind speeds equaling 0, 5, 10, 15, and 20 m/s (i.e., the last dimension of the table). Also, the Faraday rotation angle is set to 0 when computing (15). During operational processing, an adjustment to the table values is made to convert these nominal values to the actual values corresponding to a given observation. This adjustment is now discussed.

During operational processing, NCEP and other ancillary data are used to determine the actual values for τ and R_V and R_H. Also, the Faraday rotation angle ϕ_f is computed as discussed in Section 3.4. The $\mathbf{T}_{\mathbf{A},gal\_ref}$ table values are adjusted to correspond to these actual values τ, R_V, R_H and ϕ_f as follows. First, the $\mathbf{T}_{\mathbf{A},gal\_ref}$ table values are converted to brightness temperatures using the APC equation (46) below. These classical Stokes T_B' s are converted to conventional v-pol and h-pol T_B. Then the following adjustment is made:

$$T'_{BP,gal\_ref} = \tau^2 \frac{R_P}{R_{0P}} T_{BP,gal\_ref} \tag{18}$$

where the prime sign denotes the adjusted value and subscript *p* denotes polarization (*V* or *H*). The value τ is the NCEP transmittance, R_{0P} is the reflectivity computed at the nominal of 20°C and 35 psu, and R_P is the reflectivity computed at the NCEP temperature and using a reference salinity obtained from HYCOM ocean model (HYCOM, 2012). T'_{BP,gal_ref} is then converted back to classical Stokes, Faraday rotation is applied, and the inverse APC equation (i.e. A^{-1}) is applied to convert back to antenna temperature. Simulations showed that there was less error in doing the adjustment at the T_B level as compared to simply applying the adjustment to the T_A' s.

2.2.3 Direct Solar Radiation

The direct solar radiation $\mathbf{T}_{\mathbf{A},sun\_dir}$ is computed in the same way as for $\mathbf{T}_{\mathbf{A},gal\_dir}$. However, the evaluation of the integral in (5) is much simpler because the sun is a localized source and can be removed from the integral. Doing this gives

$$\mathbf{T}_{\mathbf{A},sun\_dir} = T_{B,sun}\ \frac{\Omega_{sun}}{4\pi}\mathbf{G}\left(\mathbf{b}_{sun\_direct}\right)\begin{bmatrix}2\\0\\0\\0\end{bmatrix} \tag{19}$$

where Ω_{sun} is the solid angle subtended by the sun and $\mathbf{b}_{sun\_direct}$ is the unit vector pointing from the spacecraft directly to the sun. The sun's brightness temperature is given by

$$T_{B,sun} = \frac{\lambda^2 F}{2k\Omega_{sun}} \tag{20}$$

where λ is the radiation wavelength, F is the solar flux, k is Boltzmann's constant, and Ω_{sun} is about 8.216E-5 steradians. This assumes an angular radius of 0.293^o, which is 10% greater than the optical angular radius [*Wentz*, 1978].

As with the direct galactic radiation, the computation of $\mathbf{T}_{\mathbf{A},sun\_dir}$ depends on the orbit position of the satellite and on the time of year. Tables of $\mathbf{T}_{\mathbf{A},sun\_dir}$ are generated in the same way as for $\mathbf{T}_{\mathbf{A},gal\_dir}$ and have the same structure and format, namely tasun_dir_tab(1441,1441,3,3). That is to say, tagal_dir_tab(1441,1441,3,3) and tasun_dir_tab(1441,1441,3,3) are completely analogous with one exception. For the sun table, a change in the ascending node time cannot be simply handled by an orbit phase change. Rather the table will need to be regenerated after launch (a quick process that takes about an hour) when the true ascending node time is known.

In generating tasun_dir_tab(1441,1441,3,3), we set the flux value F to 1 solar flux. Then for operational processing, the table values are multiplied by the actual flux value obtained from radio astronomy measurements. The solar flux F is a standard component of Aquarius ancillary data. (The mean noon-time solar flux is used in 20. Transient events associated with solar flares are identified with a flag.)

An analysis of the effect of solar radiation on Aquarius is given in *Wentz* [2005, 2007], which provides maps showing how the solar contamination varies during the course of a year. Typical values for $\mathbf{T}_{\mathbf{A},sun\_dir}$ are 0.05 K or less. However, because our knowledge error for antenna gain **G** in the sun's direction may be large, the calculation of $\mathbf{T}_{\mathbf{A},sun\_dir}$ is subject to error. Post-launch analyses will have to be done to determine if $\mathbf{T}_{\mathbf{A},sun\_dir}$ is indeed small enough to neglect. The processing algorithm contains an option for setting $\mathbf{T}_{\mathbf{A},sun\_dir}$ to zero.

2.2.4 Reflected Solar Radiation

The reflected solar radiation $\mathbf{T}_{\mathbf{A},sun\_ref}$ comes from the specular reflection of sunlight from a location on the Earth far away from the observation cell. The reflected sunlight enters into the far sidelodes of the antenna. Even though the gain of these far sidelobes is very small, the intensity of the sun at 1.4 GHz is so large as to make this a potential problem. The reflected

solar component can be found following the logic above for the direct component. One obtains (also see *Wentz* [1978] and *LeVine et al.* [2005], *Dinnat and Le Vine* [2008])

$$\mathbf{T}_{\mathbf{A},sun\_ref}\boldsymbol{\Psi}_{ref} = \mathbf{R}_{B,sun}\frac{\Omega'_{sun}}{4\pi}\left\langle \tau^2\mathbf{G}(\mathbf{b}) \quad (\phi) \quad \right\rangle_{ref} \tag{21}$$

where the prime sign on the sun solid angle Ω_{sun} indicates that the apparent solid angle of the sun reflecting off the spherical Earth is less than the solid angle when viewed directly. This effect is analogous to viewing an object through a convex mirror. The object will look smaller than it really is. This effect is discussed more in Section 2.2.6. The brackets in (21) denote an average over the neighborhood centered on the location of specular reflection, which is far removed from the observation footprint. The amount of averaging depends on surface roughness. For a specular (i.e., perfectly flat) surface, no averaging is required, and (21) can be evaluated for **b** pointing in the direction of the specular reflection. For high winds when the surface becomes rough, the antenna gain needs to be averaged over 5° to 10°. $\Psi(\phi)$, R and τ are defined as in (15) – (17). In the sidelobe region, the terms τ^2, $\boldsymbol{\Psi}(\phi)$, and **R** vary more slowly than **G**(**b**), and (21) can be approximated by

$$\mathbf{T}_{\mathbf{A},sun\_ref}\boldsymbol{\Psi}_{ref} = T_{B,sun}\mathbf{R}\frac{\Omega'_{sun}}{4\pi}\tau^2_{ref}\bar{\mathbf{G}}(\mathbf{b}) \quad \left(\phi_{ref}\right) \quad _{ref} \tag{22}$$

where the subscript *ref* denotes the quantity is calculated assuming a perfectly specular reflection and the overbar on the antenna gain function denotes that the antenna gain has been smoothed over a angular range to account for surface roughness.

The calculation of $R_{V,ref}$, $R_{H,ref}$, and τ_{ref} at the remote sun reflection point adds additional complexity to the modeling and algorithm. All of the ancillary data are keyed to the observation footprint which can be thousands of kilometers away from the sun reflection point. Furthermore, simulations [*Wentz,* 2005, 2007] indicate $\mathbf{T}_{\mathbf{A},sun\_ref}$ is very small, 0.01 K or less, and can probably be neglected. For now, we simply assume the reflectivity is that for a specular ocean surface at a temperature of 20°C and a salinity of 35 psu and the transmittance is set to unity. If post-launch analyses indicate $\mathbf{T}_{\mathbf{A},sun\_ref}$ has a measureable effect on the observations, then the antenna gain function **G**(**b**) will need to be revised (i.e., increased in the sidelobe region) and the retrieval algorithm will need to be modified to compute the reflectivity and atmospheric transmission at the remote location where the sun's specular reflection occurs.

Tables of $\mathbf{T}_{\mathbf{A},sun\_ref}$ are generated in the same way as for $\mathbf{T}_{\mathbf{A},sun\_dir}$ and have the same structure and format, namely tasun_ref_tab(1441,1441,3,3). The processing algorithm contains an option for setting $\mathbf{T}_{\mathbf{A},sun\_refl}$ to zero.

2.2.5 Backscattered Solar Radiation

Most of the time, the Aquarius main beam footprints will be entirely in the dark. However at the higher latitudes in the summer, the sun will be visible near the horizon, and solar radiation will impinge onto the Aquarius footprint at a grazing incidence angle. In this case, a small portion of this sunlight can be backscattered into the mainlobe of the antenna. We denote this backscatter component as $\mathbf{T}_{\mathbf{A},sun\_bak}$, and it has a magnitude on the order of 0.1 to 0.2 K when it does occur.

We use a model developed by *Dinnat and Le Vine* [2008] to specify $\mathbf{T}_{\mathbf{A},sun\_bak}$. This model parameterizes $\mathbf{T}_{\mathbf{A},sun\_bak}$ in terms of the sun's zenith angle and wind speed. $\mathbf{T}_{\mathbf{A},sun\_bak}$ is tabularized as tasun_bak_tab(161,26,3,3), where the 4 dimensions corresponds to sun zenith angle, wind speed, Stokes number, and radiometer number. The zenith angle goes from 58^o to 90^o in steps of 0.2^o, and the wind speed goes from 0 to 25 m/s in steps of 1 m/s. This table was generated assuming a solar flux, F = 264 solar flux units. For operational processing, the values from tasun_bak_tab(161,26,3,3) are multiplied by F/264, where F is the actual flux value obtained from radio astronomy measurements (RSTN noon time flux).

The $\mathbf{T}_{\mathbf{A},sun\_bak}$ tables are computed assuming a nominal surface temperature and salinity of 20^oC and 35 psu, an atmospheric transmittance of unity, and no Faraday rotation, i.e., the same nominal conditions used for the $\mathbf{T}_{\mathbf{A},gal\_ref}$ tables. During operational processing, an adjustment to the table values is made to convert these nominal values to the actual values corresponding to a given observation. This adjustment is exactly the same as described above for the reflected galactic radiation (equation 18). It should be pointed out that since $\mathbf{T}_{\mathbf{A},sun\_bak}$ is a very small term (0.1 to 0.2 K), the adjustment done by (18) has negligible effect over the ocean. The only appreciable effect of the adjustment is that over land the ratio R_P/R_{0P} becomes very small because land has a much smaller reflectivity than ocean, thereby reducing the value of $\mathbf{T}_{\mathbf{A},sun\_bak}$.

2.2.6 Reflected Lunar Radiation

At certain times each month, moonlight reflected off the ocean surface enters the mainlobe of the antenna. This phenomenon is discussed by *Dinnat et al*. [2009] and is modeled here by using a simplified antenna gain function. A simplified approach can be used because the effect occurs rarely, only is significant near the mainbeam, is small in magnitude (1 K or less). In particular, the following simplified gain pattern is adopted for the 1st and 2nd Stokes:

$$\tilde{\mathbf{G}} = \begin{pmatrix} G_{11} & G_{12} \\ G_{21} & G_{22} \end{pmatrix} 10^{-0.3\left(\frac{\xi}{\xi_0}\right)^2} \tag{23}$$

where ξ is the angle between the antenna boresight vector and the vector from spacecraft to moon specular reflection point. The angle ξ_0 is the half-power angle of the antenna pattern. Its values for the inner, middle, and outer horns are 3.04^o, 3.17^o, and 3.24^o. The values for the boresight gains G_{ij} are given in Appendix D. Equation (23) is a commonly used approximation for the gain over the mainlobe of the antenna.

The reflected lunar radiation is then given by

$$\mathbf{T}_{\mathbf{A},mon\_ref} = T_{B,moon} \frac{\Omega'_{moon}}{4\pi} \tau^2 \tilde{\mathbf{G}} \mathbf{R} \tag{24}$$

where the reflection vector **R** is given by (17) but in this case the last component, which is zero, is discarded in order to match the 2x2 rank of $\tilde{\mathbf{G}}$. . No adjustment is made for Faraday rotation, which is a small effect for the reflected lunar radiation. The terms **R** and τ are computed from the ancillary data for the observation. $T_{B,moon}$ is assumed to be 275K (Dinnat et al, 2009) and Ω'_{moon} is the apparent solid angle of the moon's reflection off the spherical earth. The relationship between the true solid angle Ω when viewed directly and the apparent solid angle Ω' when viewed as a reflection is modified by the curvature of the surface. At nadir one obtains:

$$\Omega' = \frac{\Omega}{\left(1+\frac{2s}{R_E}\right)^2} \tag{25}$$

where s is the slant path from the satellite to the point of reflection, and R_E is the Earth's radius. The expression changes slowly as a function of incidence and for Aquarius $\Omega'$for the inner, middle, and outer horns is 3.93e-05, 3.79e-05, 3.63e-05 steradians.

2.3 Earth-Only T_B Equation

The one remaining term to be specified in the forward model is $\mathbf{T}_{\mathbf{A},earth\_dir}$, which is the radiation coming just from the earth (i.e., no space radiation either direct or reflected). The one exception, the uniform cosmic background radiation that reflects off the Earth, is included in $\mathbf{T}_{\mathbf{A},earth\_dir}$. The radiation from the Earth can be written in the form:

$$\mathbf{T}_{\mathbf{A},earth\_dir} = \frac{1}{4\pi}\int_{Earth} \mathbf{G}(\mathbf{b}) \quad (\phi) \quad _{\mathbf{BE}} \frac{\partial\Omega}{\partial A} dA \tag{26}$$

where it is understood that $\mathbf{T}_{\mathbf{BE}}$ refers to the TOA brightness temperature for radiation coming just from the earth. When doing forward modeling (i.e. simulations), the integral in (26) is found by doing a very precise integration over the Earth's surface at a spatial resolution of about 1 km over the mainlobe of the antenna (a coarser resolution is used outside the mainlobe). This section discusses the Earth-only brightness temperature, $\mathbf{T}_{\mathbf{BE}}$, that appears in the kernel of the integral.

2.3.1 Theoretical Formulation

The AMSR-E ATBD [*Wentz and Meissner*, 2000] gives a detailed description of the radiative transfer equation for $\mathbf{T}_{\mathbf{BE}}$. This formulation is also applicable to Aquarius. In this section, it is more convenient to work in terms of the modified Stokes parameters (i.e., v-pol and h-pol) rather than the classical Stokes parameters. We are assuming that at 1.4 GHz, **the** 3rd and 4th Stokes parameters, which are the third and fourth elements of $\mathbf{T}_{\mathbf{BE}}$, are zero. The v-pol and h-pol components of $\mathbf{T}_{\mathbf{BE}}$ are given by

$$T_{BE,P} = T_{BU} + \tau\left[E_P T_S + T_{BP\Omega}\right] \tag{27}$$

where subscript P denotes polarization, either V or H. T_{BU} is the brightness temperature of the upwelling atmospheric radiation, τ is the atmospheric transmittance, E_P is the Earth surface emissivity, T_S is the Earth surface temperature (K), and $T_{BP\Omega}$ is the downwelling sky radiation that is scattered off the Earth surface in the direction of the observation.

The atmospheric terms can be expressed in terms of the transmittance function $\tau(s_1,s_2)$

$$\tau(s_1,s_2) = \exp\left(-\int_{s_1}^{s_2} ds\ \alpha(s)\right) \tag{28}$$

which is the transmittance between points s_1 and s_2 along the propagation path s. The term $\alpha(s)$ is the atmosphere absorption due to oxygen, water vapor, and liquid water. See *Wentz and*

Meissner [2000] for a more complete description of $\alpha(s)$. The total transmittance τ in (27) is given by

$$\tau = \tau(0, S) \tag{29}$$

where S is the slant range from the surface to the top of the atmosphere. The upwelling and downwelling atmosphere emissions are given by

$$T_{BU} = \int_0^S ds\ \alpha(s)\ T(s)\ \tau(s, S) \tag{30}$$

$$T_{BD} = \int_0^S ds\ \alpha(s)\ T(s)\ \tau(0, s) \tag{31}$$

where $T(s)$ is the air temperature profile. The scattering integral for the downwelling radiation is

$$T_{BP\Omega} = \frac{\sec\theta_i}{4\pi} \int_0^{\pi/2} \sin\theta_s d\theta_s \int_0^{2\pi} d\varphi_s (T_{BD} + \tau T_{B\cos}) \left[\sigma_{o,c}(\mathbf{k_s}, \mathbf{k_i}) + \sigma_{o,\times}(\mathbf{k_s}, \mathbf{k_i}) \right] \tag{32}$$

where θ_s is the zenith angle for the downwelling radiation impinging on the surface, and θ_i is the incidence angle for the upwelling radiation leaving the surface in the direction of the observation. The integral is over the 2π steradians of the upper hemisphere. The term $\sigma_{o,c}$ and $\sigma_{o,x}$ are the co-pol (i.e. polarization equal to P) and cross-pol (i.e. polarization orthogonal to P) bistatic normalized cross sections, which are functions of unit propagation vectors $\mathbf{k_i}$ and $\mathbf{k_s}$ that denote the direction of the upwelling and downwelling radiation, respectively. The angle φ_s is the azimuth of $\mathbf{k_s}$ relative to $\mathbf{k_i}$. These cross sections specify what fraction of power coming from $\mathbf{k_s}$ is scattered into $\mathbf{k_i}$. T_{BD} is the brightness temperature of the downwelling atmospheric radiation, and T_{Bcos} is the cosmic background plus distant galaxies radiation and equals 3 K (see Section 2.2.2).

The surface reflectivity is given by an equation similar to (32):

$$R_P = \frac{\sec\theta_i}{4\pi} \int_0^{\pi/2} \sin\theta_s d\theta_s \int_0^{2\pi} d\varphi_s \left[\sigma_{o,c}(\mathbf{k_s}, \mathbf{k_i}) + \sigma_{o,\times}(\mathbf{k_s}, \mathbf{k_i}) \right] \tag{33}$$

The surface emissivity E_P is given by Kirchhoff's law to be

$$E_P = 1 - R_P \tag{34}$$

To numerically compute $\mathbf{T_{BE}}$ from the above theoretical equations, a number of empirical models are used as is described in the next sections.

2.3.2 Empirical Approach to Specifying Atmospheric Terms

The atmospheric terms are the upwelling and downwelling brightness temperatures T_{BU} and T_{BD}, and the atmospheric transmittance τ. These are computed by numerically integrating equations (28) through (31). For operational processing, we use NCEP profiles of pressure, temperature, humidity, and liquid water to find profiles of $\alpha(s)$. The NCEP profiles are interpolated to the exact time and location of the Aquarius observations. For the oxygen

absorption component of $\alpha(s)$ we use the expressions given by *Liebe et al*. [1992]. For the water vapor absorption component of $\alpha(s)$ we use the expressions given by *Rosenkranz* [1998]. We make small modifications to both the Liebe and Rozenkranz formulations based on many years of analyzing satellite microwave observations (at Remote Sensing Systems). At 1.4 GHz, the only modification of any importance is the non-resonance continuum temperature coefficient which was changed from Liebe's exponent value of 0.8 to 1.5. This change was based on an analysis of WindSat and AMSR-E 7 GHz brightness temperatures.

2.3.3 Empirical Approach to Specifying Emissivity

The theoretical modeling of the bistatic normalized cross sections is not sufficiently advanced to provide sufficiently accurate estimates of R_P and E_P. Instead, we use the conventional approach of expressing the emissivity E_P in terms of a specular component (i.e. flat surface) and a wind-induced component:

$$E_P = E_{0P} + \Delta E_P\left(W, \varphi_r\right) \tag{35}$$

where relative wind direction φ_r is the direction of the wind relative to the azimuth angle of the Aquarius look direction. The specular component E_{0P} is computed using the Fresnel equations to obtain the reflectivity and the model of *Meissner and Wentz* [2004, 2012] for the dielectric constant of sea water.

For the wind-induced component, an empirical model derived from L-band aircraft measurements [*Yueh et al.,* 2010] is used. Yueh expresses his results in terms of an increase in brightness temperature with wind speed:

$$\begin{aligned}\Delta T_{BV}\left(W\right) &= \left(0.275 - 0.0024153\ \theta_i + 1.4026\cdot 10^{-4}\ \theta_i^2 - 2.3326\cdot 10^{-6}\ \theta_i^3\right)W \\ \Delta T_{BH}\left(W\right) &= \left(0.275 + 0.0030010\ \theta_i - 2.5181\cdot 10^{-6}\ \theta_i^2 - 6.9763\cdot 10^{-7}\ \theta_i^3\right)W\end{aligned} \tag{36}$$

where θ_i is the Earth incidence angle (deg) and W is the 10-m wind speed (m/s). We convert this to a change in emissivity as follows:

$$\Delta E_P\left(W, \phi_r\right) = \frac{\Delta T_{BP}\left(W\right)}{276.16}\frac{E_{0P}\left(T_S, S\right)}{E_{0P}\left(276.16, 35\right)} + \Phi\left(W, \phi_r\right) \tag{37}$$

where the first term is the isotropic wind-induced emissivity and the second term accounts for the wind direction variation. Yueh's measurements were done in cold water around 3°C, and hence to convert to emissivity one must divide by 276.16 K. Furthermore, to convert to the actual water temperature and salinity of the Aquarius observation, we multiply by the ratio of the actual specular emissivity to the specular emissivity corresponding to Yueh's measurements. We assume a nominal salinity of 35 psu for Yueh's measurements, although this choice has very little effect on the calculation.

The wind direction term for ΔE_P is small and is yet to be specified. As a placeholder, we are assuming the following form for the wind-direction dependence.

$$\Phi\left(W, \phi_r\right) = \left[\left(p_{1P} + p_{2P}\theta_i\right)\cos\varphi_r + \left(p_{3P} + p_{4P}\theta_i\right)\cos 2\varphi_r\right]W \tag{38}$$

where the *p* coefficients are currently set to zero. When the Aquarius Science Team has come to agreement on the specification of this term, the *p* coefficients will be updated.

For operational processing, the surface temperature T_S is currently the NCEP daily, 0.25° product and the wind speed W and direction φ_r are the NCEP 6-hour, 1° product.

2.3.4 Empirical Approach to Specifying Reflected and Scattered Radiation

The remaining term that needs to be specified is the scattering integral for the downwelling radiation: $T_{BP\Omega}$. A primary reason for computing the space radiation terms separately, as described in Section 2.2, is to facilitate the computation of $T_{BP\Omega}$. In the absence of sharply varying space terms, the integral now just contains $T_{BD}+\tau T_{Bcos}$, a small term that varies very slowly over angle. The bistatic cross section has a sharp peak in the specular direction at which $\theta_i = \theta_s$ and φ_s=180°, and over this sharp peak $T_{BD}+\tau T_{Bcos}$ varies little and can be removed from the integral. The remaining integral is simply the surface reflectivity, and hence one has

$$T_{BP\Omega} = (T_{BD} + \tau T_{B\cos})R_P \tag{39}$$

where T_{BD} and τ conveniently have the same slant path angle as T_{BU}.

2.3.5 Empirical Approach to Handling Land and Sea-Ice Observations

Although our primary focus is observations over the ocean, the formulation we have presented applies equally well to land and sea-ice observations. The only exception is that the sea-surface emissivity E_P given by (37) needs to be replaced by a land or sea-ice emissivity, with Kirchhoff's law then giving R_P. For observation of mixed surfaces, the following expressions are used

$$R_P = f_{water}R_{Pwater} + f_{land}R_{Pland} + f_{ice}R_{Pice} \tag{40}$$

$$E_P T_s = \left(1 - R_{Pwater}\right)T_{water} + \left(1 - R_{Pland}\right)T_{land} + \left(1 - R_{Pice}\right)T_{ice} \tag{41}$$

where f denotes fractional area and T denotes surface temperature. Equations (40) and (41) are then substituted into (27). The fractional land f_{land} is computed from the number of 1/12° land pixels that are within an observation footprint and this calculation is based on a static land mask. The fractional sea-ice f_{ice} comes from the NCEP operational sea-ice dataset. The fractional water is then f_{water} =1− f_{land} − f_{ice}. The reflectivities for land and sea ice are discussed in Appendix B.

3. Salinity Retrieval Algorithm

The salinity retrieval algorithm consists of a number of steps that are intended to remove the unwanted sources of radiation (galaxy, sun, moon, and Earth's atmosphere) in order to obtain just the Earth's surface emission term. A simple regression is then use to estimate salinity from the surface emission. These steps include:

1. The radiation received from the galaxy, sun, and moon is subtracted from the T_A measurements.

a. Direct radiation from the galaxy (Section 2.2.1) and Sun (Section 2.2.3) is removed. Direct radiation from the Moon is small enough to be ignored.

b. Reflected radiation from the Sun (Section 2.2.4 and 2.2.5) and Moon (2.2.6) is removed. Faraday rotation is ignored.

c. The APC is applied and (48) is used to compute a first estimate of Faraday rotation.

d. This Faraday rotation is applied to reflected galactic and Sun glint signals which are given in tables at TOA.

e. An inverse APC is applied and the two signals are subtracted from TA_TOI

2. The antenna pattern correction (APC) is applied to the residual of step 1. It removes cross-polarization contamination and corrects for sidelobes. The APC converts the top-of-the-ionosphere (TOI) antenna temperature to a brightness temperature. Then Faraday rotation is removed using the 2nd and 3rd Stokes parameters as described in (47) and (48). This provides the top-of-the-atmosphere (TOA) brightness temperature.

3. The atmospheric contributions to the TOA T_B are computed using NCEP operational fields and are removed from the TOA T_B (Section 3.5). The result is the surface emission by itself.

4. The salinity value is retrieved from the surface emission using a simple least-squares regression after a correction for wind direction.

Each of these steps is now described.

3.1 Removal of the Radiation Coming from Space

The first step in the salinity retrieval is to remove the contribution of space radiation from the antenna temperature measurement $\mathbf{T}_{\mathbf{A},mea}$. Section 2.2 lists the 6 components of space radiation and describes how they are computed during operational processing. This subtraction is represented by

$$\mathbf{T}_{\mathbf{A},earth\_dir} = \mathbf{T}_{\mathbf{A},mea} - \mathbf{T}_{\mathbf{A},gal\_dir} - \mathbf{T}_{\mathbf{A},gal\_ref} - \mathbf{T}_{\mathbf{A},sun\_dir} - \mathbf{T}_{\mathbf{A},sun\_ref} - \mathbf{T}_{\mathbf{A},sun\_bak} - \mathbf{T}_{\mathbf{A},mon\_ref} \qquad (42)$$

where we are now just left with the radiation coming directly from the Earth. Subtracting the reflected components presents a problem because after reflection they are polarized and therefore impacted by Faraday rotation which isn't known at this step in the algorithm. As a compromise, T_{A,mon_ref} is subtracted ignoring Faraday rotation. The T_{A,sun_ref} and reflected galactic radiation are subtracted after making a first estimate of the Faraday rotation as described above.

3.2 Definition of Reference Brightness Temperatures

At this point in describing the retrieval algorithm, we need to define the reference brightness temperature that we are seeking to retrieve from $\mathbf{T}_{\mathbf{A},earth\_dir}$. One possible choice is the Earth TOA T_B at boresight. However, it has been decided to define the reference brightness temperature as an average over the 3-dB Aquarius footprint since this is closer to what is actually measured. To be precise, the reference TOA T_B is defined as

$$\overline{\mathbf{T}}_{\mathbf{BE},toa} = \frac{\int\limits_{3dB\ footprt} \mathbf{T}_{\mathbf{BE},toa}\left(\overline{\theta}_i\right) dA}{\int\limits_{3dB\ footprt} dA} \tag{43}$$

where the integral is over the 3-dB footprint and the overbar denotes the average over the footprint. The 3-db footprint is defined as that part of the Earth integral for which the angle between the boresight vector $\mathbf{b_0}$ and the look vector $\mathbf{b}$ is less than 3.07°, 3.17°, and 3.24° for the inner, middle, and outer horns, respectively. We further specify that when doing the footprint averaging, the incidence angle is held to a constant value $\overline{\theta}_i$, which is the gain-weighted average incidence angle given by

$$\overline{\theta}_i = \chi\theta_{i,boresight} \tag{44}$$

where $\theta_{i,boresight}$ is the boresight incidence angle, and χ is 1.00177, 1.00186, 1.00148 for the inner, middle, and outer horns, respectively. This adjustment is so small that it probably is not needed and one could simply use the boresight incidence angle for $\overline{\theta}_i$. By definition $\overline{\mathbf{T}}_{\mathbf{BE},toa}$ is a characteristic of the Earth scene being viewed (an average value), and is independent of the radiometer antenna except that the regime of averaging is the 3db antenna footprint. This is the parameter that the algorithm is designed to retrieve.

Because Faraday rotation is important at L-band, there are two brightness temperatures that also must be defined: Brightness temperature at the top of the ionosphere and at the top of the atmosphere. The top-of-the-ionosphere (TOI) reference brightness temperature is denoted by $\overline{\mathbf{T}}_{\mathbf{BE},toi}$ and is related to the brightness temperature at the top of the atmosphere, T_{BE_toa} by the Faraday rotation:

$$\overline{\mathbf{T}}_{\mathbf{BE},toi} = \mathbf{T}\left(\phi_f\right)^{-}_{\mathbf{BE},toa} \tag{45}$$

3.3 Estimation of Top-of-the-Ionosphere Brightness Temperature

Now that we have defined our reference T_B, we must estimate its value given the antenna temperature $\mathbf{T}_{\mathbf{A},earth\_dir}$. In principle we are seeking the solution of the integral equation (26): That is, given the measurement, $\mathbf{T}_{\mathbf{A},earth\_dir}$, the goal is to determine $\overline{\mathbf{T}}_{\mathbf{BE},toi}$. Since it is not possible to directly invert the integral, other means are required. We use the following method.

Simulations using the forward algorithm are performed to produce a year of simulated $\mathbf{T}_{\mathbf{A},earth\_dir}$. This represents about 25 million observations for each horn at intervals of 1.44 seconds. The following regression is then assumed.

$$\hat{\mathbf{T}}_{\mathbf{BE},toi} = \mathbf{A}\cdot\mathbf{T}_{\mathbf{A},earth\_dir} \tag{46}$$

where $\mathbf{A}$ is a 3 by 3 matrix called the antenna pattern correction (APC) matrix, and the 'hat' on $\mathbf{T}_{\mathbf{BE},toi}$ denotes that this is an estimated quantity as compared to the true value. In addition to providing $\mathbf{T}_{\mathbf{A},earth\_dir}$, the simulation also provides the true value of $\overline{\mathbf{T}}_{\mathbf{BE},toi}$. The standard least-squares method is used to find the APC matrix $\mathbf{A}$ that minimizes the variance of $\hat{\mathbf{T}}_{\mathbf{BE},toi} - \overline{\mathbf{T}}_{\mathbf{BE},toi}$.

When deriving the APC matrix, **A**, simulated observations that contain sea ice or that are a mixture of land and water are excluded. That is to say, regression (46) is only done for observations that are totally land or totally water, i.e., uniform scenes. It was decided not to train the regression with extremely non-uniform scenes, which pose many difficulties when trying to relate antenna temperatures to brightness temperatures.

Considering all complexities of the integral equation (26), it is not obvious if a simple regression like (46) will perform adequately. To evaluate its performance, we compute the rms value of $\hat{\mathbf{T}}_{\mathbf{BE},toi} - \overline{\mathbf{T}}_{\mathbf{BE},toi}$ using all the simulated observations. These statistics were done separately for all-ocean and all-land observations, but the same APC matrix was used for both. Over the ocean, the rms for v-pol and h-pol ranged from 0.05 to 0.08 K. Over land, the rms values were considerably higher, ranging from 1 to 2 K. The higher land values are due to the land T_B having more variability. A small number of land observations having very large variability show errors of 10-20 K, which have a great influence on the rms statistics. These results show that the APC regression (46) works well for uniform scenes, like the ocean. Non-uniform scenes present a problem for the APC, which is probably unavoidable.

Experiments were made deriving the APC just with ocean observations since this is the primary focus. There was a slight improvement when the ocean-only APC was applied to the ocean observations, but the improvement was very small compared to the over all performance of 0.05 to 0.08 K, and a decision was made to stay with the ocean+land APC, which is trained over the full range of T_A.

The largest error in the APC is with respect to the 3rd Stokes parameter for the outer horn, for which the ocean-only observations exhibit an rms of 0.2K. However, the 3rd Stokes parameter is just used for Faraday rotation correction, and the mapping of this error into the estimate of the top-of-the-atmosphere (TOA) T_B is very small.

The 0.05 to 0.08 K performance of the APC is of some concern, given the demanding requirements for Aquarius brightness temperature accuracy. Some experiments were made in an attempt to improve its performance, such as using an ocean-only APC, using separate APC for ascending and descending orbit segments, and adding higher order terms to (46). These attempts helped slightly, but not enough to warrant their implementation. However, with more time and analysis, we do think that there is the potential for improving the APC performance.

3.4 Correction for Faraday Rotation

The next step in the retrieval is a correction for Faraday rotation. *Yueh* [2000] gave a detailed description of the Faraday rotation problem and proposed measuring the 3rd Stokes parameter to remove its effect, as we will now discuss. Faraday rotation is removed by applying the following expression.

$$\hat{\mathbf{T}}_{\mathbf{BE},toa} = \mathbf{T}\left(-\phi_f\right)\hat{}_{\mathbf{BE},toi} \tag{47}$$

If one assumes that the 3rd and 4th Stokes parameters due to radiation from the Earth surface are negligibly small, one may set the 3rd Stokes parameter in $\overline{\mathbf{T}}_{\mathbf{BE},toa}$ to zero and obtain the Faraday rotation angle:

$$\phi_f = \frac{1}{2}\arctan\left(\frac{\hat{T}_{BE,toi,3}}{\hat{T}_{BE,toi,2}}\right) \tag{48}$$

where the last subscript denotes Stokes number. Substituting (48) into (47) one obtains the TOA T_B

$$\begin{aligned}\hat{T}_{BE,toa,1} &= \hat{T}_{BE,toi,1} \\ \hat{T}_{BE,toa,2} &= \sqrt{\left[\hat{T}_{BE,toi,2}\right]^2 + \left[\hat{T}_{BE,toi,3}\right]^2}\end{aligned} \tag{49}$$

Wentz [2006] analyzed the error between the estimated $\hat{\mathbf{T}}_{\mathbf{BE},toa}$ and the true $\overline{\mathbf{T}}_{\mathbf{BE},toa}$ using this procedure with a more realistic antenna. The rms difference was about 0.04 K for ocean v-pol and h-pol observations. This analysis (*Wentz,* 2006) used an antenna gain pattern obtained from numerical computation at JPL of the pattern expected from the Aquarius antenna (also see Le Vine et al, 2007). Since then, the computer model pattern has been replaced by a pattern measured using a scale-model of the antenna system (e.g. OMT, feed and reflector) which has considerably larger cross-polarization terms. These large cross-polarization terms result in larger error when doing the APC. The rms value of $\hat{\mathbf{T}}_{\mathbf{BE},toa} - \overline{\mathbf{T}}_{\mathbf{BE},toa}$ obtained using the scale-model pattern is 0.05 to 0.08 K, nearly all of which is due to the APC error as mentioned in the previous section.

3.5 Removal of Atmospheric Effects

In this subsection we switch over to using the modified Stokes parameters (v-pol and h-pol) rather than the classical Stokes parameters for $\hat{\mathbf{T}}_{\mathbf{BE},toa}$, and these two components are denoted simply as $T_{BE,P}$, where subscript P denotes polarization (either V or H). This step in the retrieval algorithm is intended to remove the effect of the atmosphere. This is done by inverting (27) to yield surface emission $T_{BE,sur}$.

$$T_{BE,P,sur} \equiv E_P T_S = \frac{T_{BE,P} - T_{BU}}{\tau} - T_{BP\Omega} \tag{50}$$

Substituting (39) in (50) gives

$$T_{BE,P,sur} \equiv E_P T_S = \frac{T_{BE,P} - T_{BU}}{\tau} - (T_{BD} + \tau T_{B\cos})R_P \tag{51}$$

Noting that $R_P = 1 - E_P$, (51) can be rewritten as

$$T_{BE,P,sur} = \left[\frac{\dfrac{T_{BE,P} - T_{BU}}{\tau} - (T_{BD} + \tau T_{B\cos})}{T_S - (T_{BD} + \tau T_{B\cos})}\right] T_S \tag{52}$$

where the bracketed term is the surface emissivity.

The atmospheric terms for the upwelling and downwelling brightness temperature T_{BU} and T_{BD}, and the atmospheric transmittance τ are computed by numerically integrating equations (28) through (31) along the boresight ray. For operational processing, we use NCEP profiles of pressure, temperature, humidity, and liquid water to find profiles of $\alpha(s)$. The NCEP profiles are interpolated to the exact time and location of the Aquarius observations. See Section 2.3.2 for details. The auxiliary SST field used is the Reynolds OI product which is based on IR data [*Reynolds, 2007*]. The land surface temperature T_S currently comes from the NCEP daily, 0.25^o product. After launch other sources for *Ts* will be considered such as the AMSR-E and WindSat microwave only retrieval of sea surface temperature. T_{Bcos} is a constant 3 K (cosmic background plus a constant contribution from celestial sources). Given these ancillary data, (52) can be calculated to yield the surface emission brightness temperature. Note that this calculation of $T_{BE.P,sur}$ is done for all surface types (ocean, land, sea-ice, and mixed) as described in Section 2.3.5.

3.6 Estimation of Salinity Given Surface Emission Brightness Temperature

Over the ocean, the surface emission $T_{BE.P,sur}$ depends on surface temperature, T_S, surface salinity, S, surface roughness, and Earth incidence angle, θ_i. For now, we are parameterizing the surface roughness effect simply as a function of the wind measured 10 meters above the surface, where W denotes the speed (m/s) and φ_r denotes the relative wind direction. The wind direction effect is given by (38) and is first removed from the surface T_B.

$$T'_{BE,P,sur} = T_{BE,P,sur} - \Phi\left(W, \phi_r\right) T_S \tag{53}$$

where the prime sign denotes that the wind direction effect is removed.

The algorithm for estimating sea-surface salinity from the surface emission $T'_{BE,P,sur}$ is described by Wentz and Yueh [2004]. The algorithm takes the form

$$S = s_0\left(\theta_i, t_S\right) + s_1\left(\theta_i, t_S\right) T'_{BE,V,sur} + s_2\left(\theta_i, t_S\right) T'_{BE,H,sur} + s_3\left(\theta_i, t_S\right) W \tag{54}$$

where θ_i is the incidence angle, t_S is the sea-surface temperature in °C ($T_S = t_S + 273.15$), and W is sea-surface wind speed (m/s). The s coefficients are functions of θ_i and t_S and are in tabular form. The algorithm is trained by deriving a set of s coefficients that minimize variance between the salinity S given by (54) and the true salinity. Separate sets of s coefficients are found for 251 incidence angles going from 25° to 50° in 0.1° steps and 451 t_S values going from –5°C to 40°C in 0.1°C steps. These 251×451 tables are interpolated to the specified value for θ_i and t_S.

The algorithm training requires that $T'_{BE,P,sur}$ be computed over the full range of S, T_S, W and θ_I using equations (35) through (38). Note that this is the only point in the retrieval algorithm where the specification of the dielectric constant of sea water [*Meissner and Wentz*, 2004, 2012], and the wind-induced emissivity [*Yueh et al.*, 2010] comes into play. Using a different dielectric model or a different wind model would result in a different set of s coefficients.

For a given θ_i and t_S, the relationship between surface brightness temperature and salinity is close to linear, but not quite. If necessary, equation (54) will be supplemented by adding a second stage algorithm that will remove any error caused by the deviation from linearity. This type of two-stage algorithm has proven very effective in handling the non-linearity characteristic

in the AMSR-E retrievals. However, any such fine tuning should wait until the L-band wind model (i.e., equations 36-38) is known more precisely. We expect that about 6-months after launch an improved wind model will be developed, and we can then take a closer look equation (54).

Note that in training the algorithm, a different amount of noise can be applied to the v-pol and h-pol T_B to account for the actual error in these T_B retrievals. Also, an analogous algorithm can be developed that uses the sum of v-pol and h-pol T_B to eliminate residual Faraday rotation error. The salinity retrievals from the V+H algorithm can be compared to those coming from the dual-polarization algorithm to test if there is any residual Faraday rotation error. This type of experimenting will be done after launch.

Another alternative to (54) is to subtract the wind-induced T_B correction $\Delta T_{BP}(W)$ from $T_{BE,P,sur}$ prior to the salinity retrieval. This is the approach used for the algorithm derived during the WISE experiments [*Camps et al.*, 2002]. However as said above, it is probably best to wait until we have the improved post-launch wind model before trying these different alternatives.

The salinity retrieval is very sensitive to errors in T_S and W. The pre-launch version of the algorithm currently uses the daily Reynolds IR 0.25^o product for T_S and the NCEP 6-hour, 1^o product for W. After launch, other sources for T_S and W will be considered. Microwave retrievals of sea surface temperature from WindSat could possibly prove to be more accurate than the NCEP sea surface temperatures. Also, at some point, we expect to start using the wind speed derived from the Aquarius microwave scatterometer.

3.7 Calculation of Expected Antenna Temperature

Section 2.3 gives the formulation necessary to compute the 'earth-only' TOA T_B. The inputs to the formulation (SST, wind, atmospheric terms, etc.) are all described above with the exception of salinity, which in the above treatment was considered the retrieval. In order to compute an expected TOA T_B, we need to have some reasonable value for salinity. For a reference salinity field we use the 3-dimensional global ocean general circulation model based on the HYbrid Coordinate Ocean Model called "HYCOM" (HYCOM, 2012). The HYCOM data are made available typically within two days after the model run via servers located at the Center For Ocean-Atmospheric Prediction Studies (COAPS), Florida State University (FSU). Given this salinity value along with all the ancillary data needed to retrieve salinity, an expected TOA T_B is computed. Using the Faraday rotation angle computed by (48), the inverse of equation (47) is applied to convert the expected TOA T_B to an expected TOI T_B. The inverse $\mathbf{A}^{-1}$ of the APC matrix is then used to convert the TOI T_B to an expected antenna temperature value. See equation (46). Finally, all of the various space radiation terms are added back in according to equation (42), thereby obtaining an expected T_A measurement denoted as $T_{A,exp}$.

If the salinity retrieval value was used instead of the reference salinity field, $T_{A,exp}$ would closely match $T_{A,mea}$. The two would not be exactly the same because both v-pol and h-pol are used to retrieve salinity, and hence the retrieval problem is over-determined. Notwithstanding this, the difference $T_{A,mea} - T_{A,exp}$ is essentially a mapping into T_A space of the difference of the retrieved salinity minus the reference field salinity. Early in the calibration and validation activity, during which we expect relatively large (>0.5 K) calibration errors in $T_{A,mea}$, the

difference $T_{A,mea}$ - $T_{A,exp}$ can be used to remove these calibration errors. Of course one needs to be careful not to over tune using this difference, else the retrieved salinity will be too closely tied to the reference salinity field. This question of over tuning will be more important later on in the calibration processes after the initial large errors are removed.

3.8 Correction for Land Entering the Antenna Sidelobes

A correction for land entering the antenna sidelobes when the Aquarius observation is close to land is found by running the Aquarius on-orbit simulator. Simulations have shown that the salinity retrieval degrades quickly as the footprint approaches land (closer than 400 km). This land-contamination error, which occurs because the land is much warmer than the ocean is described by *Wentz* [2006]. The error due to land entering the sidelobes, is defined as

$$\Delta \mathbf{T}_{\mathbf{BE},toa} = \hat{\mathbf{T}}_{\mathbf{BE},toa} - \overline{\mathbf{T}}_{\mathbf{BE},toa} \tag{55}$$

which is the difference of the TOA T_B, estimated from the observed (i.e. measured) signal as given by equation (47), minus the true TOA T_B coming from the antenna main beam and defined by (43). The Aquarius simulator is used to produce a table of $\mathbf{\Delta T}_{\mathbf{BE},toa}$. This table is stratified according to the spacecraft nadir longitude (1440 elements in 0.25° increment), the spacecraft position in orbit (1440 elements in 0.25° increment), month (12 elements), polarization (v-pol, h-pol), and horn (inner, middle, and outer) and takes the form Tb_land_correction(1440,1440,12,2,3). $\mathbf{\Delta T}_{\mathbf{BE},toa}$ is found by linearly interpolating the table to the exact spacecraft position. The interpolated value of $\mathbf{\Delta T}_{\mathbf{BE},toa}$ is then subtracted from the actual TOA T_B coming from equation (47) in the retrieval, and then the retrieval process proceeds as usual.

The second dimension of spacecraft position in orbit is the same as described in Section 2.2.1. The third dimension of month is required to account for seasonal variability in the land brightness temperatures, although this effect is fairly minor. Note that the land correction tables do not consider sea ice. We suggest that the land correction only be done when the fractional land contamination exceeds 0.0005 to avoid unnecessarily adding noise for observations very far from land. Also, it is to be emphasized that this "land correction" is only correcting for the presence of land in the antenna sidelobes. When it approaches the main beam, a different type is probably necessary.

Other methods for the removal on land contamination are also being investigated. One method for sidelobe removal that has been applied to radiometers on JASON and ENVISAT is to divide the integration (e.g. in equation 26) into additional sectors such as the on-Earth sidelobes to obtain a mainbeam brightness temperature, and to eventually deconvolve the mainbeam brightness temperature [*Brown,* 2005].

4. Outstanding Issues

Once Aquarius is in operation and we begin receiving real L-band antenna temperatures, we expect that there will be some major revisions such as rederiving the wind-induced emissivity. The determination of the dependence of the emissivity on wind speed should be straightforward, however determining the wind direction dependence will be more challenging. Currently the

wind directional term for $\Phi(W,\phi_r)$ is given by (38), with all the *p* coefficients set to zero.

With respect to evaluating the specular emissivity, research is underway at the George Washington University and at the Polytechnic University of Catalonia to refine the *Klein and Swift* [1977] model function for emissivity at L-band that relates the brightness temperature to sea surface temperature and salinity. After launch, the salinity retrievals using the Meissner-Wentz dielectric constant model can be compared with those using the alternative dielectric constant model. This type of experimenting is done by recomputing the *s* coefficients in (54) using a different dielectric constant model. Similar experimenting can be done with different wind-induced emissivity models.

5. References

Brown, S., Modified APC Algorithm for JMR/TMR/AMR, *JPL JMR Memo*, 27 Jan 2005

Camps, A., et al., Sea surface emissivity observations at L-band: First results of the Wind and Salinity Experiment WISE 2000, *IEEE Transactions on Geoscience and Remote Sensing, 40*(10), 2117-2130, 2002.

Cox, C., and W. Munk, Measurement of the roughness of the sea surface from photographs of the sun's glitter, *J. Opt. Soc. Amer., 44*(11), 838-850, 1954.

Dinnat, E.P. and D.M. Le Vine, Impact of sun glint on salinity remote sensing: An example with the Aquarius radiometer, *IEEE Transactions on Geoscience and Remote Sensing*, 46(10), 3137-3150, 2008.

Dinnat, E. P., S. Abraham, D. M. Le Vine, P. de Matthaeis and D. Jocob, Effect of emission from the moon on remote sensing of sea surface salinity: An example with the Aquarius radiometer, *IEEE Geoscience and Remote Sensing Letters, 6*(2), 239-243, 2009.

HYCOM, 2012: The Hybrid Coordinate Ocean Model: http://hycom.org. The output used here is from Center for Ocean-Atmospheric Prediction Studies (COAPS) at Florida State University.

Klein, L. A. and C. T. Swift, An improved model for the dielectric constant of sea water at microwave frequencies, *IEEE Transactions on Antennas and Propagation, AP-25*, 104-111, 1977.

LeVine, D. M., S. Abraham, The effect of the ionosphere on remote sensing of sea surface salinity from space: Absorption and emission at L-band, *IEEE Transactions on Geoscience and Remote Sensing*, 40 (4), 771-782, April, 2002

LeVine, D. M., S. Abraham, Galactic noise and passive microwave remote sensing from space at L-band, *IEEE Transactions on Geoscience and Remote Sensing*, 42 (1), 119-129, 2004.

Le Vine, D.M., S. Abraham, F. Wentz and G.S.E. Lagerloef, Impact of the sun on remote sensing of sea surface salinity from space, *Proceedings of IGARSS*, Seoul Korea, vol. 1, 288-291, 2005.

Le Vine, D.M., S. D. Jacob, E. P. Dinnat, P. de Matthaeis, and S. Abraham, The influence of antenna pattern on Faraday rotation in remote sensing at L-band, *IEEE Transactions on Geoscience and Remote Sensing*, 45(9), 2737-2746, 2007a.

Le Vine, D.M,, G. S. E. Lagerloef, F. R. Colomb, S. H. Yueh, and F. A. Pellerano, Aquarius: An instrument to monitor sea surface salinity from space, *IEEE Trans. Geosci. Remote Sens.*, vol. 45, no. 7, pp. 2040–2050, Jul. 2007b.

Le Vine, D.M., E. P. Dinnat, S. Abraham, P. de Matthaeis and F. Wentz, The Aquarius Simulator and Cold Sky Calibration, *IEEE Transactions on Geoscience and Remote Sensing*, 49(9), 3198-3210, 2011.

Liebe, H. J., P. W. Rosenkranz and G. A. Hufford, Atmospheric 60-GHz oxygen spectrum: New laboratory measurements and line parameters, *Journal of Quantitative Spectroscopy & Radiative Transfer, 48*, 629-643, 1992.

Meissner, T. and F. J. Wentz, The complex dielectric constant of pure and sea water from microwave satellite observations, *IEEE Trans. on Geoscience and Remote Sensing, 42*(9), 1836-1849, 2004.

Meissner, T. and F. J. Wentz, 2012, The Emissivity of the Ocean Surface Between 6 and 90 GHz Over a Large Range of Wind Speeds and Earth Incidence Angles, *IEEE Trans. on Geoscience and Remote Sensing, 50*, in print, DOI 10.1109/TGRS.2011.2179662.

Meissner, T. et al., 2012, The Aquarius Salinity Retrieval Algorithm, Proceedings of the 12th Specialist Meetings on Microwave Radiometry and Remote Sensing of the Environment, Rome, Italy, IEEE Catalog Number CFP12MIC-CDR.

Randa, J. et al, Recommeded terminology for Microwave Radiometry, NIST Technical Note 1551, U.S. Gov Printing Office, August, 2008.

Reynolds, R., et al., 2007, Daily High-Resolution-Blended Analyses for Sea Surface Temperature, *J. of Climate, 20*, 5473 – 5496.

Rosenkranz, P., Water vapor microwave continuum absorption: A comparison of measurements and models, *Radio Science, 33*(4), 919-928, 1998.

Wentz, F. J., Cox and Munk's Sea Surface Slope Variance, *J. Geophysical Res. 81*(9), 1607-1608, 1976.

Wentz, F. J., The forward scattering of microwave solar radiation from a water surface, *Radio Science 13* (1), 131-138, February 1978.

Wentz, F. J., A model function for ocean microwave brightness temperatures, *J. Geophys. Res,. 88*, pp 1892 - 1908, 1983.

Wentz, F. J., Simulation of Solar Contamination for Aquarius, *RSS Technical Report 060305*, June 3, 2005.

Wentz, F. J., The Estimation of TOA T_B from Aquarius Observations, *RSS Technical Report 013006*, January 30, 2006.

Wentz, F. J., Update to Simulation of Solar Contamination for Aquarius: Results from Scale-Model Antenna Patterns, *RSS Technical Report 020907*, February 9, 2007.

Wentz, F. J. and T. Meissner, Algorithm Theoretical Basis Document (ATBD), Version 2, AMSR Ocean Algorithm, *RSS Tech. Report 121599A-1*, November 2, 2000.

Wentz, F. J., and S. H. Yueh, Salinity Error due to Surface Roughness Effects, *RSS Memorandum 121504*, December 15, 2004.

Wilheit, T.T. and A. T. C. Chang, An algorithm for retrieval of ocean surface and atmospheric parameters from the observations of the scanning multichannel microwave radiometer, *Radio Science, 15(3)*, pp 525 - 544, 1980.Yueh, S. H., Estimates of Faraday rotation with passive microwave polarimetry for microwave remote sensing of Earth surfaces, *IEEE Transactions on Geoscience and Remote Sensing, 38*(5), 2000.

Yueh, S. H., S. J. Dinardo, A. G. Fore and F. K. Li, Passive and Active L-Band Microwave Observations and Modeling of Ocean Surface Winds, *IEEE Transactions on Geoscience and Remote Sensing, 48*(8), 3087-3100, 2010.

6. Appendix A. Reflected Galactic Brightness Temperature

In section 2.2.2, the reflected galactic radiation $\mathbf{T}_{\mathbf{A},\text{gal\_ref}}$ in terms of antenna temperature is given as an integral over the antenna pattern. Inside the integral is the term $\mathbf{T}_{\mathbf{B},\text{gal\_ref}}$ which represents the brightness temperature of the reflected galactic radiation at the top of the atmosphere. This Appendix gives the formulation for $\mathbf{T}_{\mathbf{B},\text{gal\_ref}}$.

The rough ocean surface is modeled as a collection of tilted facets, with each facet acting as an independent specular reflector. The formulation for this model is given by *Wentz* [1978]. Equation (7) in *Wentz* [1978] can be rewritten as

$$T_B(\mathbf{k_s}, \mathbf{P_s}) = \tau^2 \iint d\Omega_i k_i^z \Gamma(\mathbf{k_i}; \mathbf{k_s}, \mathbf{P_s}) T_B(\mathbf{k_i}) \tag{A1}$$

where $T_B(\mathbf{k_s}, \mathbf{P_s})$ is the top of the atmosphere scattered galactic radiation propagating in the direction of the unit vector $\mathbf{k_s}$ having polarization $\mathbf{P_s}$. The vector $\mathbf{k_i}$ is the downward propagation vector from the galaxy. $T_B(\mathbf{k_i})$ is the brightness temperature of the galaxy coming from direction $\mathbf{k_i}$. It comes from the *Le Vine and Abraham* [2004] map with the 3 K floor value subtracted out (see Section 2.2.2). The term $\Gamma(\mathbf{k_i}; \mathbf{k_s}, \mathbf{P_s})$ is the scattering function defined below. The atmospheric transmittance is denoted by τ. We assume that the transmittance is the same for the downwelling and upwelling radiation. The value along the boresight ray is used and assumed to be the same at all points in the integral (e.g. over the footprint of the antenna). This assumption is dictated by the coarse spatial resolution (100 km) of the NCEP data used to compute τ

The integral is over differential solid angles $d\Omega_i$. In *Wentz* [1978] the differential solid angle was given in terms of the x,y,z components of $\mathbf{k_i}$.

$$d\Omega_i = \frac{dk_i^x \, dk_i^y}{dk_i^z} \tag{A2}$$

where the z axis is aligned with the normal to the Earth's geoid. In doing the integration it is convenient to transform the integral using the following Jacobian:

$$d\Omega_i = 4(\mathbf{n} \cdot \mathbf{z})^3 (\mathbf{k_s} \cdot \mathbf{n}) dz_u dz_c \tag{A3}$$

where $\mathbf{n}$ is the unit surface normal vector for a particular facet, z_u and z_c and the two slopes of the facet in the upwind and crosswind directions, and unit vector $\mathbf{z}$ is the normal to the Earth's geoid.

$$T_B(\mathbf{k_s}, \mathbf{P_s}) = \tau^2 \int\int dz_u dz_c \, 4(\mathbf{n} \cdot \mathbf{z})^3 (\mathbf{k_s} \cdot \mathbf{n})(\mathbf{k_i} \cdot \mathbf{z}) \Gamma(\mathbf{k_i}; \mathbf{k_s}, \mathbf{P_s}) T_B(\mathbf{k_i}) \tag{A4}$$

The scattering function is give by [*Wentz*, 1978]

$$\Gamma(\mathbf{k_i}; \mathbf{k_s}, \mathbf{P_s}) = \frac{P_z(z_u, z_c)}{4(\mathbf{k_s} \cdot \mathbf{z})(\mathbf{k_i} \cdot \mathbf{z})(\mathbf{n} \cdot \mathbf{z})^4} \Upsilon \tag{A5}$$

$$\Upsilon = |\mathbf{P_s^*} \cdot \mathbf{H_s}|^2 |R_h|^2 + |\mathbf{P_s^*} \cdot \mathbf{V_s}|^2 |R_v|^2 \tag{A6}$$

where P_z is the probability distribution function (pdf) for the facet slopes, and $\mathbf{V_s}$ and $\mathbf{H_s}$ are the local v-pol and h-pol unit vectors of a particular facet. The terms R_v and R_h are the v-pol and h-pol reflectivities for the facet. The superscript * denotes complex conjugate. For specifying R_v and R_h we use the *Meissner and Wentz* [2004, 2012] dielectric constant for the specular component and the *Yueh et al.* [2010] model for the wind-induced component (Equations 36). Note that there is a small inconsistency in doing this because the Yueh wind-induced component

already includes to some degree the roughening effect due to facet tilting. Since the Yueh wind-induced component also includes the effect of sea foam and Bragg scattering, it is difficult to separate all the effects and we thought it was better to include the wind-induced component as compared to simply using the specular reflectivity in (A6). For computing the scattering of galactic radiation this issue is minor, having about a 2% effect on the computation, which translates to a worst case uncertainty of 0.1 K or less.

Combining terms we then get

$$T_B(\mathbf{k_s}, \mathbf{P_s}) = \tau^2 \int\int dz_u dz_c \, T_B(\mathbf{k_i})(\mathbf{k_s} \cdot \mathbf{n}) \frac{P_Z(z_u, z_c)}{(\mathbf{k_s} \cdot \mathbf{z})(\mathbf{n} \cdot \mathbf{z})} \Upsilon \tag{A7}$$

The brightness temperature classical stokes vector appearing in equation (15) is then given by

$$\mathbf{T}_{\mathbf{B},gal\_ref} = \begin{bmatrix} T_B(\mathbf{k_s}, \mathbf{v}) + T_B(\mathbf{k_s}, \mathbf{h}) \\ T_B(\mathbf{k_s}, \mathbf{v}) - T_B(\mathbf{k_s}, \mathbf{h}) \end{bmatrix} \tag{A8}$$

where **v** and **h** are the v-pol and h-pol vectors referenced to the Earth's geoid and $\mathbf{k_s}$ is in the direction of the differential solid angle for the integral shown in (15).

The key issue in computing $T_B(\mathbf{k_s}, \mathbf{P_s})$ is what to use for the facet slope pdf. The classic *Cox and Munk* [1956] experiment, which measured the ocean sun glitter distribution, clearly showed that to first order the slope pdf is Gaussian. Higher order pdf moments were also observed (skewness and peakedness), and the rms slopes in the upwind direction were found to be somewhat higher than the downwind direction. For L-band microwave observations the higher wavelength components of surface roughness, which are small relative to the L-band wavelength of 21 cm, do not contribute to the facet tilting. Thus when applying the Cox and Munk results to low-frequency microwave observations, one must reduce the Cox and Munk rms slopes. This is a well accepted fact and there have been many papers written on the subject [e.g. *Wentz*, 1983; *Wilheit and Chang*, 1980]. However, the exact value of the reduction factor and how it varies with radiation wavelength is still uncertain. For the AMSR-E Algorithm Theoretical Basis Document [*Wentz and Meissner*, 2000], the following was used to specify the facet slope pdf:

$$P_z(z_u, z_c) = \frac{e^{-\frac{z_u^2 + z_c^2}{\sigma^2}}}{\pi\sigma^2} \tag{A9}$$

where an isotropic slope distribution was assumed. The total facet slope variance is given by

$$\begin{aligned} \sigma^2 &= 5.22 \times 10^{-3} W \qquad f \geq 37 GHz \\ \sigma^2 &= 5.22 \times 10^{-3} W \left[1 - 0.00748 (37 - f)^{1.3} \right] \qquad f < 37 GHz \end{aligned} \tag{A10}$$

where f denotes frequency (GHz) and W is the 10-meter wind speed used elsewhere in this report. For frequencies above 37 GHz, the Cox and Munk clean surface slope variance is used. For frequencies below 37 GHz, the slope variance is decreased as explained in *Wentz and Meissner* [2000]. More recently *Meissner and Wentz* [2012] , the above expression has been replaced by a slightly different expression based on more analysis of satellite data.

$$\sigma^2 = 0.0029 W \log_{10}(2f) \qquad f < 100 GHz \tag{A11}$$

This is the expression we use for calculating the tables of for $\mathbf{T_B}_{,gal\_ref}$. At frequencies above 32 GHz, this expression gives a slope variance somewhat higher than Cox and Munk, consistent with the fact that the Cox and Munk value probably represents a lower bound on the true slope variance [*Wentz*, 1976]. For f = 1.41 GHz, both (A10) and (A11) represent approximately a 50% reduction in the Cox-Munk clean surface slope variance. This reduction is similar to the Cox and Munk oil-slick results. Oil was poured on the ocean surface to dampen out the capillary waves. The oil-slick results also indicated a slope distribution that was nearly isotropic, consistent with (A9), as compared to the clean surface results that indicated an anisotropic distribution.

The above expressions are then used to compute the term $\mathbf{T_B}_{,gal\_ref}$ that appears in the equation for reflected galactic radiation $\mathbf{T_A}_{,gal\_ref}$. This represents a four-fold integral that needs to be calculated with a numerical precision of better than 0.1 K. To compute all the T_A tables described in Section 2.2.2 required 48 3-GHz processors running for 2 months.

7. Appendix B. Land and Sea-Ice Reflectivities

I. Introduction:

When the surface is not ocean, the formulation outlined in the text is used but with the surface reflectivity, R_p, in (34) and (39) replaced by a value appropriate for the surface. In the case of mixed surfaces, the following expressions are used:

$$R_P = f_{water} R_{Pwater} + f_{land} R_{Pland} + f_{ice} R_{Pice} \quad (40)$$

$$E_P T_s = (1 - R_{Pwater}) T_{water} + (1 - R_{Pland}) T_{land} + (1 - R_{Pice}) T_{ice} \quad (41)$$

where f denotes fractional area and T_s denotes surface temperature. For example, (40) is used in (39) and (41) is used in (27) to obtain the signal from the surface upwelling to the radiometer when the surface is other than ocean. The fraction of land, f_{land}, is computed using the number of $1/12^o$ pixels identified as land that are within an observation footprint. The land mask used in this calculation is static (i.e. these calculations do not have to be done in real time). The fraction of sea-ice, f_{ice}, comes from the NCEP operational sea-ice dataset. The fraction of water is then $f_{water} = 1 - f_{land} - f_{ice}$. The surface temperatures are the surface temperatures given by NCEP.

These are the only categories in the current simulator. However, if the land surface temperature is less than 0 C (freezing), the algorithm assumes frozen ground and uses a fixed dielectric constant (relative permittivity) $\varepsilon = 1.73 + i0.00012$, which is based on snow with a density of 0.4 (Ulaby et al, Fig E.26 and E.28), to compute the reflectivity. Details of the reflectivity used for land and ice are discussed below. The reflectivity for the water fraction is as described in Section 2.2 and 2.3. Non-ocean water bodies are treated the same as ocean: NCEP wind speed is used in same way as over ocean and the algorithm uses the reference salinity field when it is available. If not, the salinity is set to 35 psu (although zero would probably be a better choice for non-ocean water bodies).

The beginning point in the calculation is the reflectivity of a smooth surface. This is obtained using the Fresnel reflection coefficients for a plane surface tangent to the geodetic reference surface at the point where the ray from the spacecraft antenna intersects this reference surface. The reflectivities are denoted R_v,h and given by:

$$R\_v = \left| \frac{\cos\theta - \sqrt{\varepsilon - \sin^2\theta}}{\cos\theta + \sqrt{\varepsilon - \sin^2\theta}} \right|^2 \quad \text{(h-pol)} \qquad \text{B1}$$

$$R\_h = \left| \frac{\varepsilon \cos\theta - \sqrt{\varepsilon - \sin^2\theta}}{\varepsilon \cos\theta + \sqrt{\varepsilon - \sin^2\theta}} \right|^2 \quad \text{(v-pol)} \qquad \text{B2}$$

In the equations above, ε is the relative dielectric constant of the surface material (e.g. land) at the intersection point and θ is the angle of incidence measured with between the incident ray and the local normal to the surface. The parameters needed to determine the reflectivity (e.g. soil moisture and temperature) are obtained from the NCEP data.

II. Reflectivity for Land

In the case of land surfaces, the reflectivity in (A1-2) is modified to account for surface roughness and a possible vegetation canopy.

A. Roughness

The effect of roughness is to decrease the reflectivity of the smooth surface. Experiments (e.g. Wang and Choudhury, 1981; Pellerin et al, 2003) suggest that the effect can be modeled with a relationship in the form:

$$R\_rough\_v,h \rightarrow R\_v,h \exp[-h_s] \qquad \text{B3}$$

where h_s is an empirical value related to the roughness and R_v,h are given in A1-2. One choice for the roughness parameter is $h_s = (4 \pi \sigma / \lambda)^2 \cos(\theta)^2$ where σ is the standard deviation of the height of the surface roughness (e.g. Ulaby et al, 1986; section 11-2.3). Given a lack of adequate information about surface roughness on a global scale, the current version of the forward model employs a fixed value, $h_s = 0.3$, as suggested by Pellerin et al, 2003 (see their Appendix and their Eqn B3). Assuming a constant means that any dependence on incidence angle and polarization mixing have been neglected. Also, (B3) applies to field-scale roughness and the effect topography is not addressed.

B. Vegetation Canopy

Assuming that the vegetation canopy is a homogeneous layer, the effect of the canopy can be modeled in the form:

$$Rveg\_v,h \rightarrow R\_v,h \exp[-2\tau \sec(\theta)] \qquad \text{B4}$$

where τ is the optical depth of the layer. Jackson and Schmugge (1991) have shown that the optical depth can be related to the structure of the vegetation and the vegetation water content, W, in the form:

$$\tau = b\,W. \qquad \text{B5}$$

The structure parameter, b, depends on the type of vegetation and perhaps polarization. Given limited information on a global scale, the approach adopted for the Aquarius simulator is to assume a constant value for b:

$$b = 0.15 \qquad \text{B6}$$

and to obtain the vegetation type and water content from ECOCLIMAP (Masson et al, 2003) as suggested by Pellerin et al (2001):

Table I: Vegetation Water Content

Surface Classification		Vegetation Water Content
Bare		0
Crops		0.5 LAI
Grass		0.5 LAI
Rain Forest		6
Deciduous Trees		4
Conifer Trees		3

The LAI and the canopy classification for each pixel are obtained from ECOCLIMAP. The data is given as the fraction of each cover type. Hence, using the table above for the water content :

$$W = (0.0)\,F\_bare + 0.5\,(F\_grass + F\_crop)\,LAI + \qquad \text{B7}$$
$$+ 6\,F\_rainForest + 4\,F\_deciduous + 3\,F\_conifer$$

where F denotes the fraction of each cover type at the center of each footprint (antenna boresight).

C. Total

The effects of roughness and vegetation canopy are combined to obtain an effective reflectivity for land:

$$R\_land\_v,h = R\_v,h \exp[-hs - 2\tau \sec(\theta)] \quad \text{B8}$$

$$= R\_v,h \exp[-0.3 – 0.3\{ 0.5 (F\_grass + F\_crop) LAI + 6 F\_rainForest + 4 F\_deciduous + 3 F\_conifer \} \sec(\theta)]$$

III. The relative dielectric constant, ε

The parameter, ε, in (B1-2) is the relative dielectric constant of the material at the surface. In the case of ocean, the model developed by Meissner and Wentz (2004) is currently being used (Section 2.3.3). In the case of land, at 1.4l3 GHz, the model developed by Dobson et al (1985, Eqn 28) as reported in Ulaby et al (1986; Vol III, Eqn E111 and E112) has been adopted.

$$\varepsilon = 1 + (r_b/r_{ss})*(eps_{SS}^{alph} - 1) + (W^{beta})*((4.9 + 74.1/(1 - 6*(f/f_o)*i))^{alph}) – W \quad \text{B9}$$

where W is the volumetric soil moisture, f is frequency, and

f_o = 18.64 GHz = relaxation frequency of pure water;

r_b = soil bulk density in g/cm3 (density of the naturally occurring soil/air mixture);

r_{ss} = density of solid soil (g/cm3)

The parameters “alpha” and “beta” are tuned to obtain the best fit to measurements:

alpha = 0.65

beta = 1.09 – 0.11 S + 0.18 C

S and C are the fractions by weight of the sand and clay, respectively, in the soil. The value of alpha = 0.65 fits well for all soil types and the expression for beta has been taken from Ulaby et al (Vol III, pg 2103).

Since accurate information about soil parameters is not available on a global scale, fixed values have been assumed for these parameters. The following choices have been made:

r_b = 1.3

r_{ss} = 2.65

alpha = 0.65

beta = 1.09

All of these parameters are static. The only parameters which change in the computations for land are the surface temperature, Ts, and the value for soil moisture, W, both of which are taken from the NCEP data.

IV. Ice

A. Sea Ice

The fraction of sea-ice, f_{ice}, comes from the NCEP operational sea-ice dataset. For lack of better information, the relative permittivity of sea ice has been assumed to be fixed:

$$\varepsilon = 3.0 - i\,0.1$$

This is a crude guess based on data for freshwater ice (Ulaby et al, pg 2026-2027).

B. Frozen Land (Snow)

As mentioned above, if the surface temperature (from NCEP) is 0 or less, the land category is assigned a fixed ε based on the dielectric constant of snow:

$$\varepsilon = 1.73 - i\,0.00012$$

V. References

Dobson, M.C., F.T. Ulaby, M.T. Hallikainen and M.A. El-rayes, 1985: Microwave dielectric behavior of wet soil-part II: dielectric mixing models, *IEEE Trans. Geosci. Remote Sens.*, **GE-23**, 35-45.

Jackson, T.J. and T.J. Schmugge, 1991: Vegitation effects on the microwave emission of soils, *Remote sens. environ.* , **36**, 203-212.

Masson, V., J.L. Champeaux, F. Chauvin, C. Meriguet and R. Lacaze, 2003: A global database of land surface parameters at 1-km resolution in mereorological and climate models, *J. Clim.*, **16**, 1261-1282.

Meissner, T. and F. J. Wentz, 2004, The complex dielectric constant of pure and sea water from Microwave satellite observations, *IEEE Trans. on Geoscience and Remote Sensing, 42*(9), 1836-1849.

Meissner, T. and F. J. Wentz, 2012, The Emissivity of the Ocean Surface Between 6 and 90 GHz Over a Large Range of Wind Speeds and Earth Incidence Angles, *IEEE Trans. on Geoscience and Remote Sensing, 50*, in print, DOI 10.1109/TGRS.2011.2179662.

Pellarin, T., J.P. Wigneron, J.C. Calvet and P. Waldteufel, 2003: Two-year global simulation of L-band brightness temperatures over land, *IEEE Trans. Geosci. Remote Sens.*, **41**, 2135-2139.

Ulaby, F.T., R.K. Moore and A.K. Fung, 1986: *Microwave Remote Sensing: Active and Passive, Volume 3: from theory to applications*, Artech Inc., Norwood, 2162 pp.

Wang, J.R.and B.J. Choudhury, 1981, Remote Sensing of Soil Moisture Content Over Bare Field at 1.4 GHz Frequency, J. Geophys. Research, Vol 86, C6, pp 5277-5282, June

8. Appendix C: Dielectric Constant of Soil (Addendum to Appendix B)

Several models, available in the literature, for the dielectric constant of soil at L-band as a function of soil moisture were compared. The models considered are:

I. Modified Dobson: From Dobson et al, 1985 as presented by Ulaby et al, 1986 (Vol III, Eqn E111 and E112:

$$eps = 1 + (rb/rss)(epsSS^{alph} - 1) + (W^{beta})(4.9 + 74.1/(1 - i\,6\,f/fo))^{alph} - W$$

epsrD = real[$eps^{(1/alph)}$];

epsiD = imag[$eps^{(1/alph)}$];

where W is the volumetric soil moisture, S and C are sand and clay sand fractions, respectively, and:

beta = 1.09 - 0.11*S + 0.18*C;

alph = 0.65

rb = 1.3 (soil bulk density)

rss = 2.65 (density of solid soil)

epsSS = 4.7 (dielectric constant of dry soil)

II. Hallikainen: From Hallikainen et al, 1985, Part I (Table II)

The following coefficient matrices are taken from Table II:

coefReal1p4 = [2.862 -0.012 0.001 3.803 0.462 -0.341 119.006 -0.500 0.633];

coefIm1p4 = [0.356 -0.003 -0.008 5.507 0.044 -0.002 17.753 -0.313 0.206];

Using these coefficients, the real part of the dielectric constant is:

$$epsrH = (2.862 - 0.012*S + 0.001*C) + (3.803 + 0.462*S - 0.341*C)*W + (119.006 - - 0.500*S + 0.633*C)*W^2;$$

and the imaginary part of the dielectric constant is:

$$epsiH = (0.356 - 0.003*S - 0.008*C) + (5.507 + 0.044*S - 0.002*C)*W + (17.753 - 0.313*S + 0.206*C)*W^2;$$

and the dielectric constant itself is:

epsH = epsrH + i*epsiH;

III. Wang: From Le Vine and Kao, 1997 (Eqn 4) which was provided by Wang based on research publish in Wang, 1980

The real and imaginary parts of the dielectric constant are:

epsrL = 3.1 + 17.36*W + 63.12*W^2; Real part

epsiL = 0.031 + 4.65*W + 20.42*W^2; Imaginary part

and eps = epsrL + i* epsiL

IV. Experiment: Data taken from Ulaby et al, 1986, Figure E.47. Two cases were used for reference:

A. Silt Loam (curve 4):

Sand = 17.2%

Silt = 63.8

Clay = 19.0

epsr_sl = [2.5, 3.0, 4.25, 6.0, 8.75, 11.5 15.0 19.63, 24.5, 29.75];

epsi_sl = [0, .45, .75, 1.38, 2.13, 2.75, 3.5, 4.38, 5.5, 6.3];

B. Silt Clay (curve 5):

Sand = 5.0%

Silt = 47.6

Clay = 47.4

epsr_sc = [2.5, 3.0, 4.0, 5.5, 7.5, 10.5, 13.75, 17.75, 22.25, 27.38, 33.25];

epsi_sc = [0, .5, 1.0, 1.5, 2.13, 3.0, 4.0, 5.0, 6.25, 7.75, 9.25];

V. Comparison:

A. Dielectric Constant

The figures below show the real and imaginary part of the dielectric constant predicted by each model together with the measured values at L-band as a function of volumetric soil moisture.

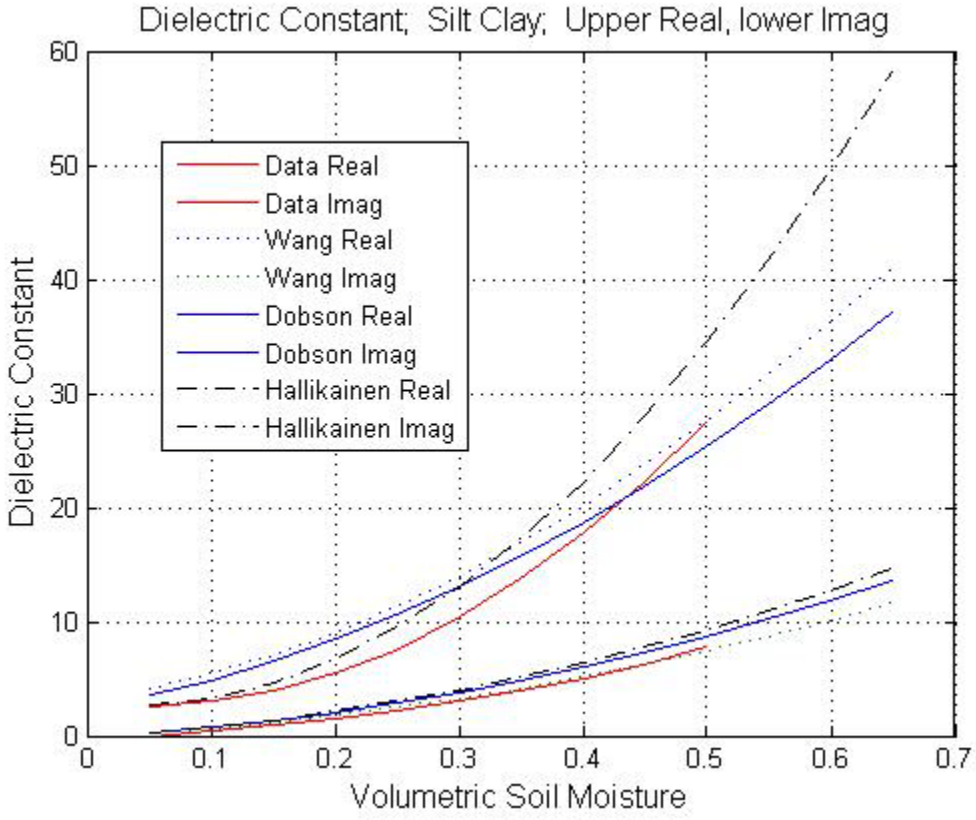

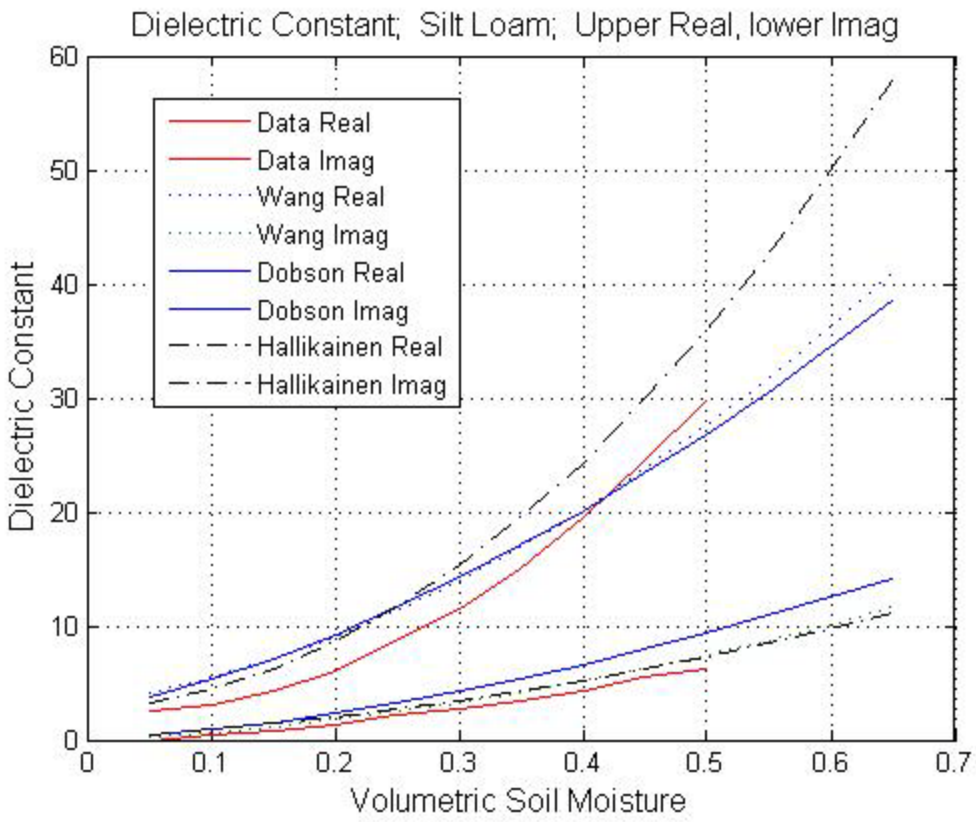

The larger values are the real part and the group with smaller values are the imaginary part. The Wang and modified Dobson model are similar and also fit well the measured imaginary part. The Hallikainen model follows the shape of the data as a function of soil moisture but is offset with respect to the measured values especially at higher values of Mv. It predicts larger values for both the real and imaginary parts.

B. Brightness Temperature

The brightness temperature is plotted below as a function of soil moisture for the two soil types and at incidence angles corresponding to the inner and outer beams of the Aquarius radiometers. The two angles, 28.7 and 45.6 degrees are the local incidence angles (i.e. with respect to the normal to the surface).

A. Silt Loam

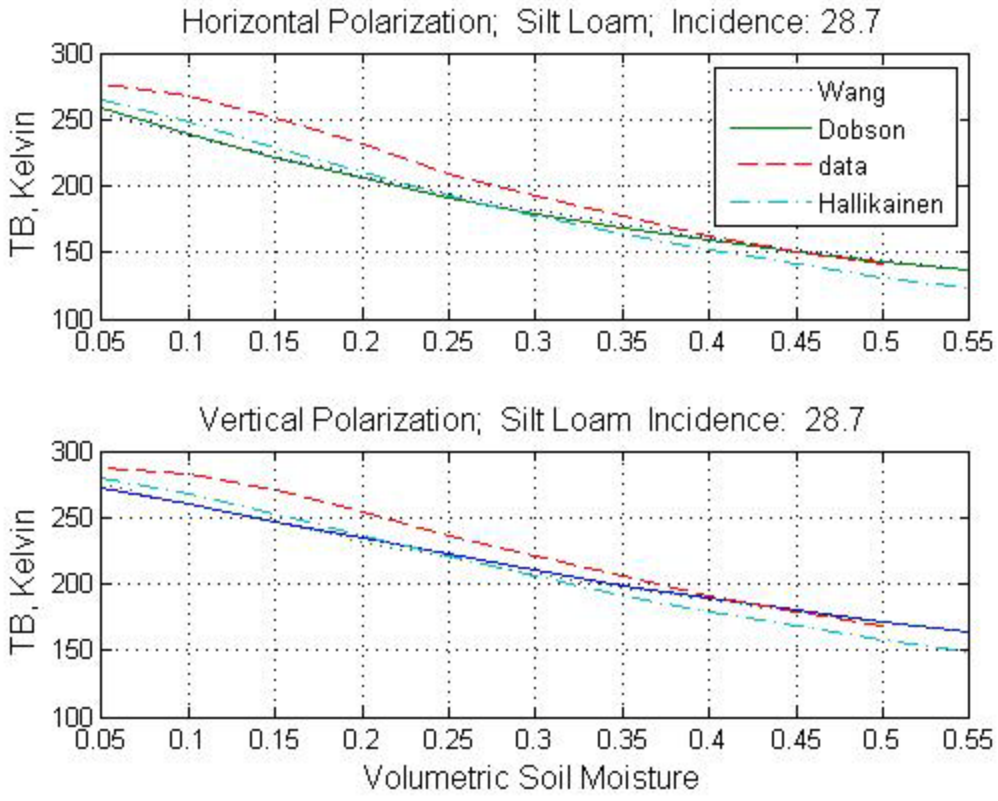
Horizontal Polarization; Silt Loam; Incidence: 28.7
TB, Kelvin
300
250
200
150
100
0.05
0.1
0.15
0.2
0.25
0.3
0.35
0.4
0.45
0.5
0.55
Wang
Dobson
data
Hallikainen
Vertical Polarization; Silt Loam Incidence: 28.7
TB, Kelvin
Volumetric Soil Moisture

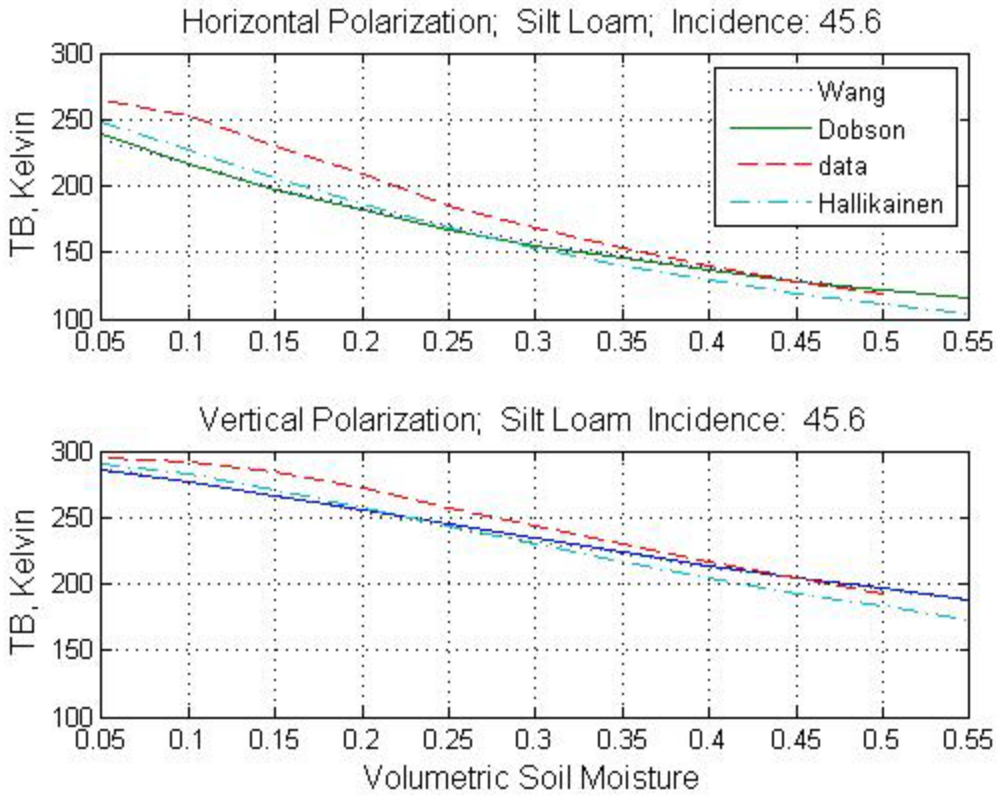
Horizontal Polarization; Silt Loam; Incidence: 45.6
TB, Kelvin
300
250
200
150
100
0.05
0.1
0.15
0.2
0.25
0.3
0.35
0.4
0.45
0.5
0.55
Wang
Dobson
data
Hallikainen
Vertical Polarization; Silt Loam Incidence: 45.6
TB, Kelvin
Volumetric Soil Moisture

B. Silt Clay

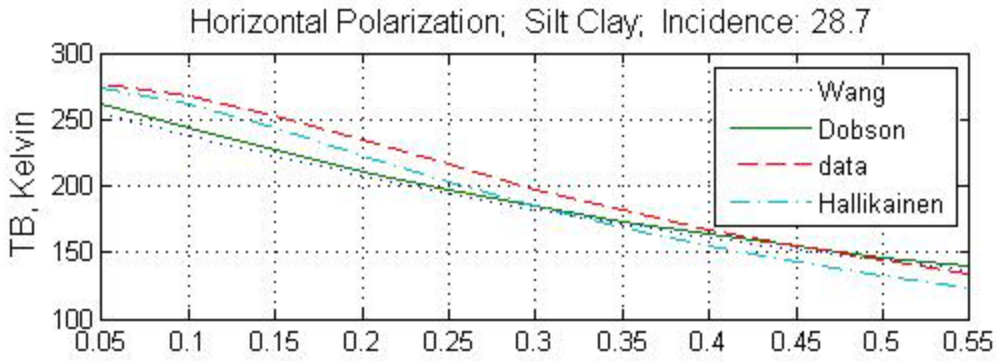
Horizontal Polarization; Silt Clay; Incidence: 28.7
TB, Kelvin
300
250
200
150
100
0.05
0.1
0.15
0.2
0.25
0.3
0.35
0.4
0.45
0.5
0.55
Wang
Dobson
data
Hallikainen

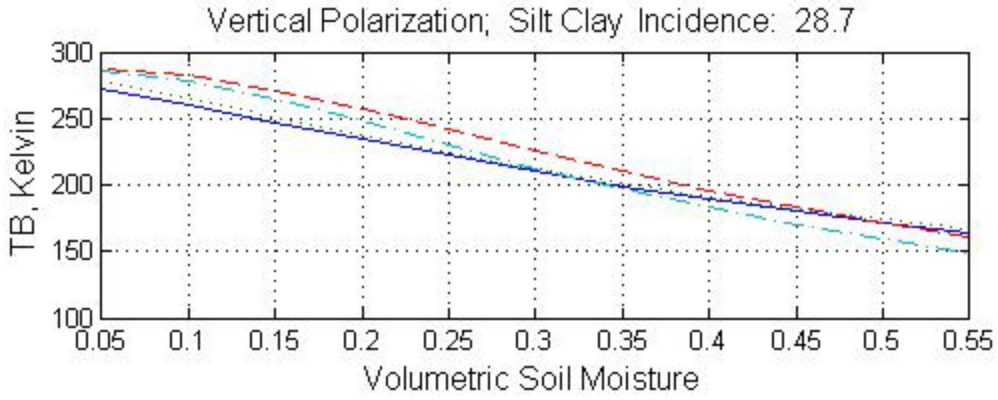
Vertical Polarization; Silt Clay Incidence: 28.7
TB, Kelvin
300
250
200
150
100
0.05
0.1
0.15
0.2
0.25
0.3
0.35
0.4
0.45
0.5
0.55
Volumetric Soil Moisture

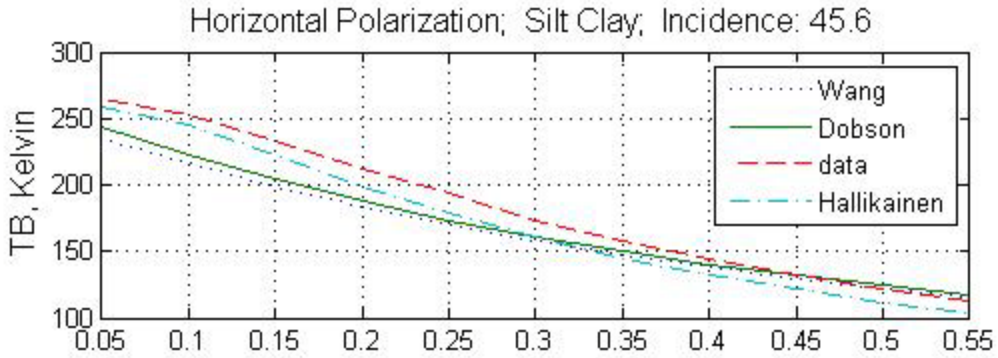
Horizontal Polarization; Silt Clay; Incidence: 45.6
TB, Kelvin
300
250
200
150
100
0.05
0.1
0.15
0.2
0.25
0.3
0.35
0.4
0.45
0.5
0.55
Wang
Dobson
data
Hallikainen

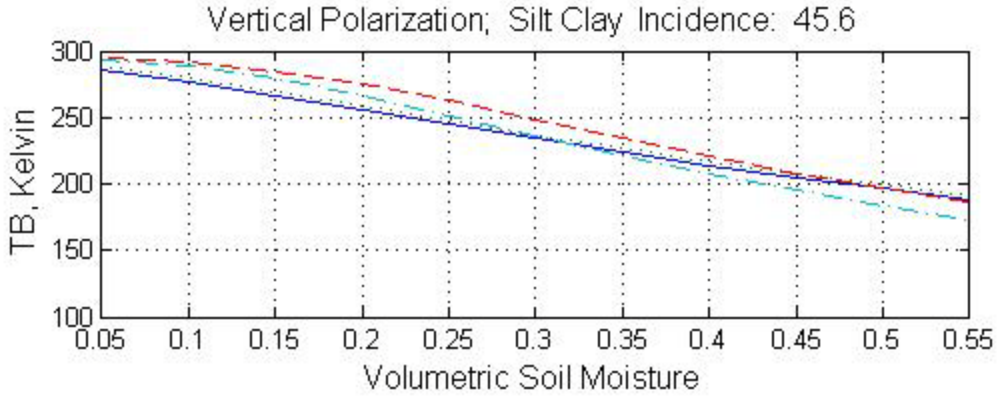
Vertical Polarization; Silt Clay Incidence: 45.6
TB, Kelvin
300
250
200
150
100
0.05
0.1
0.15
0.2
0.25
0.3
0.35
0.4
0.45
0.5
0.55
Volumetric Soil Moisture

The TB predicted by the three models are close in the case of silt-loam. In this case, the Hallikainen model does a bit better for dry soil and the other two models do better for wet soil. In the case of silt-clay, the Hallikainen model is noticeably better for dry soil and fits the shape of the curve of the data well. The other two models again do a bit better for wet soil. In both cases, there is little difference between the Wang and modified Dobson models.

V. Conclusion

The comparison presented here is a comparison of model and data for only one group of measurements. The Hallikainen model is the result of a fit to this data and so it is expected that it would perform better than the other two models. As far as the models are concerned, the Wang and modified Dobson model are very close. The Hallikainen model follows the shape of the dielectric constant and brightness temperature well, but is biased somewhat high for wet soils (for the dielectric constant). All the models under-predict the TB for dry soils, but the Hallikainen model is better. The Wang and modified Dobson model do better for wet soil.

V. References

Dobson, M.C., F.T. Ulaby, M.T. Hallikainen and M.A. El-rayes, 1985: Microwave dielectric behavior of wet soil-part II: dielectric mixing models, *IEEE Trans. Geosci. Remote Sens.*, **GE-23**, 35-45.

Hallikainen, M, F.T. Ulaby, M.C. Dobson, M. El-Rayes and L.K. Wu, 1985, "Microwave Dielectric Behavior of Wet Soil – Part I: Empirical Models and Experimental Observations", IEEE Trans. Geosci. Remote Sensing, GE-23, pp. 25-34, Table II.

Le Vine, D.M. and M. Kao, "Effects of Faraday rotation on microwave on remote sensing from space at L-band," in *Proc. IGARSS*, Aug. 1997, 857 vol. 1, pp. 377–379. See Eqn 4.

Ulaby, F.T., R.K. Moore and A.K. Fung, 1986: *Microwave Remote Sensing: Active and Passive, Volume 3: from theory to applications*, Artech Inc., Norwood, 2162 pp.

J. Wang, "The dielectric properties of soil-water mixtures at microwave frequencies," *Radio Sci.*, vol. 15, no. 5, pp. 977–985, 1980.

Comments:

1. The Dobson model for the dielectric constant includes a term which is supposed to apply at 1.4GHz (Dobson et al, 1985). This term is dependent on conductivity. In order to include it, the following expression should be added to the term in the brackets and raised to the power "alph" in Equation B9:

$$- \; i\, W^{beta-1}\, (sig\_eff / (2*pi*f*eo))(1 - rb/rss)$$

where

$$sig\_eff = -1.645 + 1.939\ rb - 0.02013\ S + 0.01594\ C$$

Calculations were made with and without this term with no noticeable difference.

2. The soil moisture in (B9) is volumetric. Much of the data is in terms of gravimetric soil moisture:

Mg = gravimetric soil moistsure = weight of water in the soil / weight of dry soil
= (Wwet – Wdry)/ Wdry
= usually expressed as a fraction.

Mv = volumetric soil moisture = Volume of water in soil / Volume dry soil
= Vwater / Vdry = (Wwater / rwater) / (Wdry/rdrysoil)
= (Wwater / Wdry) rb (using rwater = 1 and rdrysoil = rb by definition)
= usually expressed in %.
= (Wwet – Wdry) rb / Wdry
= Mg rb
= 1.3 Mg for our choice of parameters

9. Appendix D. Gain Coefficients for Reflected Lunar Radiation

The following table gives the boresight gains used to compute reflected lunar radiation as specified by equation (23).

Horn	G_{11}	G_{12}	G_{21}	G_{22}
Inner	74.41968	-0.47552	-0.42802	74.36780
Middle	70.84354	0.13980	0.12591	70.82498
Outer	65.86123	-0.58609	-0.52414	65.78670